bioRxiv preprint doi: https://doi.org/10.1101/2022.10.06.510775; this version posted October 7, 2022. The copyright holder for this preprint (which was not certified by peer review) is the author/funder, who has granted bioRxiv a license to display the preprint in perpetuity. It is made available under aCC-BY-NC-ND 4.0 International license.

Direct estimation of genome mutation rates from pedigrees in free-ranging baleen whales

Authors:

Marcos Suárez-Menéndez[1]*†, Martine Bérubé[1,2]†, Fabrício Furni[1], Vania E. Rivera-León[1], Mads-Peter Heide-Jørgensen[3], Finn Larsen[4], Richard Sears[5], Christian Ramp[5,6], Britas Klemens Eriksson[1], Rampal S. Etienne[1], Jooke Robbins[2]‡, Per J. Palsbøll[1,2]*‡

Affiliations:

[1] Groningen Institute for Evolutionary Life Sciences, University of Groningen, Groningen, The Netherlands

[2] Center for Coastal Studies, Provincetown, Massachusetts, United States of America

[3] Greenland Institute of Natural Resources, Nuuk, Greenland

[4] National Institute of Aquatic Resources, Kongens Lyngby, Denmark

[5] Mingan Island Cetacean Study Inc., St. Lambert, Quebec, Canada

[6] Scottish Oceans Institute, University of St. Andrews, St. Andrews, United Kingdom

†,‡ These authors contributed equally to this work.

*Corresponding authors: Marcos Suárez Menéndez, Email: m.suarez.menendez@rug.nl and Per J. Palsbøll, Email: palsboll@gmail.com

Abstract

Current low germline mutation rate (μ) estimates in baleen whales have greatly influenced research ranging from assessments of whaling impacts to evolutionary cancer biology. However, the reported rates were subject to methodological errors and uncertainty. We estimated μ directly from pedigrees in natural populations of four baleen whale species and the results were similar to primates. The implications of revised μ values include pre-exploitation population sizes at 14% of previous genetic diversity-based estimates and the conclusion that μ in itself is insufficient to explain low cancer rates in gigantic mammals (i.e., Peto's Paradox). We demonstrate the feasibility of estimating μ from whole genome pedigree data in natural populations, which has wide-ranging implications for the many ecological and evolutionary inferences that rely on μ.

bioRxiv preprint doi: https://doi.org/10.1101/2022.10.06.510775; this version posted October 7, 2022. The copyright holder for this preprint (which was not certified by peer review) is the author/funder, who has granted bioRxiv a license to display the preprint in perpetuity. It is made available under aCC-BY-NC-ND 4.0 International license.

Main

Adaptive evolution is ultimately driven by the appearance of novel genotypes, which in turn are a result of *de novo* germline mutations (*DNMs*) and recombination. The rate (μ, i.e., the probability of a nucleotide substitution per site per generation) of *DNMs* varies considerably among taxonomic groups. Multiple causes have been proposed to explain observed differences in μ (*1*), such as selection on μ itself, or a reflection of differences in physiological and cellular processes (e.g., metabolic rates, and DNA repair mechanisms). In addition, μ is a central parameter in evolution and population genetic inference and necessary when converting genetic estimates into more intuitive quantities, such as time and abundance. Most estimates of μ are obtained from DNA-based phylogenies (μ_{PHY}) with dated branching points (e.g., from fossil records); an approach which is subject to multiple sources of error and uncertainty (*2*). However, the advent of inexpensive whole genome sequencing methodologies has enabled direct estimation of μ from pedigrees of individuals (μ_{PED}), which relies on fewer assumptions and μ_{PED} is readily comparable among species providing an opportunity to test current hypotheses regarding the differences in μ and revisit key findings and hypotheses based on μ_{PHY}.

Baleen whales (*Mysticeti*, *Cetacea*) include the largest and longest-lived mammals; aspects which have been invoked as the cause of low observed estimates of μ_{PHY} in this group of mammals. Their gigantic body size results in relatively low metabolic rates (compared to smaller-bodied mammals) and thus a lower expected μ (*3*). Indeed, estimates of μ_{PHY} in both the nuclear and mitochondrial (mt) genome of baleen whales were lower than similar estimates for smaller-bodied mammals, such as primates (*4*). The lower μ_{PHY} observed in baleen whales has, in turn, been hypothesized to explain low cancer rates in baleen whales, part of a phenomenon known as Peto's Paradox (*5*, *6*). However, the cause and consequences of such lower μ_{PHY} have been the subject of considerable debate (*4*, *7*). Baleen whales were historically subjected to substantial human exploitation on a global scale from industrial whaling; but the full extent of that depletion remains unknown. Estimates of μ_{PHY} were applied to estimates of pre-exploitation abundance based on current levels of genetic diversity in some whale species (*8*, *9*), yielding pre-exploitation abundance estimates 4-10 times higher than results obtained by other means (*10*). These high estimates of pre-exploitation whale abundance further imply that the historic oceans supported a much larger biomass of whales and prey.

Estimates of μ_{PED} in the nuclear genome have so far only been obtained from ~20 vertebrate species, mainly primates and model species raised in captivity (table S1). In contrast, estimates of μ_{PED} in natural populations are rare and so far confined to a single small group of individuals in small distinct population in only three species (a quartet of platypus, *Ornithorhynchus anatinus*, inhabiting the same creek, *11*, a septet in a single wolf, *Canis lupus*, pack, *12*, and a known three-generation pedigree of collared flycatchers, *Ficedula albicollis*, in a study population, *13*). We demonstrate that μ_{PED} estimates are readily obtained by combining genetic relatedness analysis with genome sequencing in difficult-to-sample natural populations of non-model species without any prior pedigree knowledge.

We combined genetic parentage exclusion analysis (based on microsatellite genotypes) with molecular sex determination and mt DNA sequences to identify offspring and parents trios among free-ranging North Atlantic blue (*Balaenoptera musculus*), fin (*Balaenoptera physalus*), bowhead (*Balaena mysticetus*) and humpback (*Megaptera novaeangliae*) whales. Except for humpback whales, no prior pedigree information was available. However, despite a relatively low sampling probability in some species (e.g., ~4% for the bowhead whale, *14*),

bioRxiv preprint doi: https://doi.org/10.1101/2022.10.06.510775; this version posted October 7, 2022. The copyright holder for this preprint (which was not certified by peer review) is the author/funder, who has granted bioRxiv a license to display the preprint in perpetuity. It is made available under aCC-BY-NC-ND 4.0 International license.

subsequent whole genome sequencing confirmed the initial identification of offspring and parent trios. Our estimate of μ_{PED} in baleen whales was based on *DNMs* detected in eight parent-offspring trios: one each in blue, fin and bowhead whales and five in humpback whales.

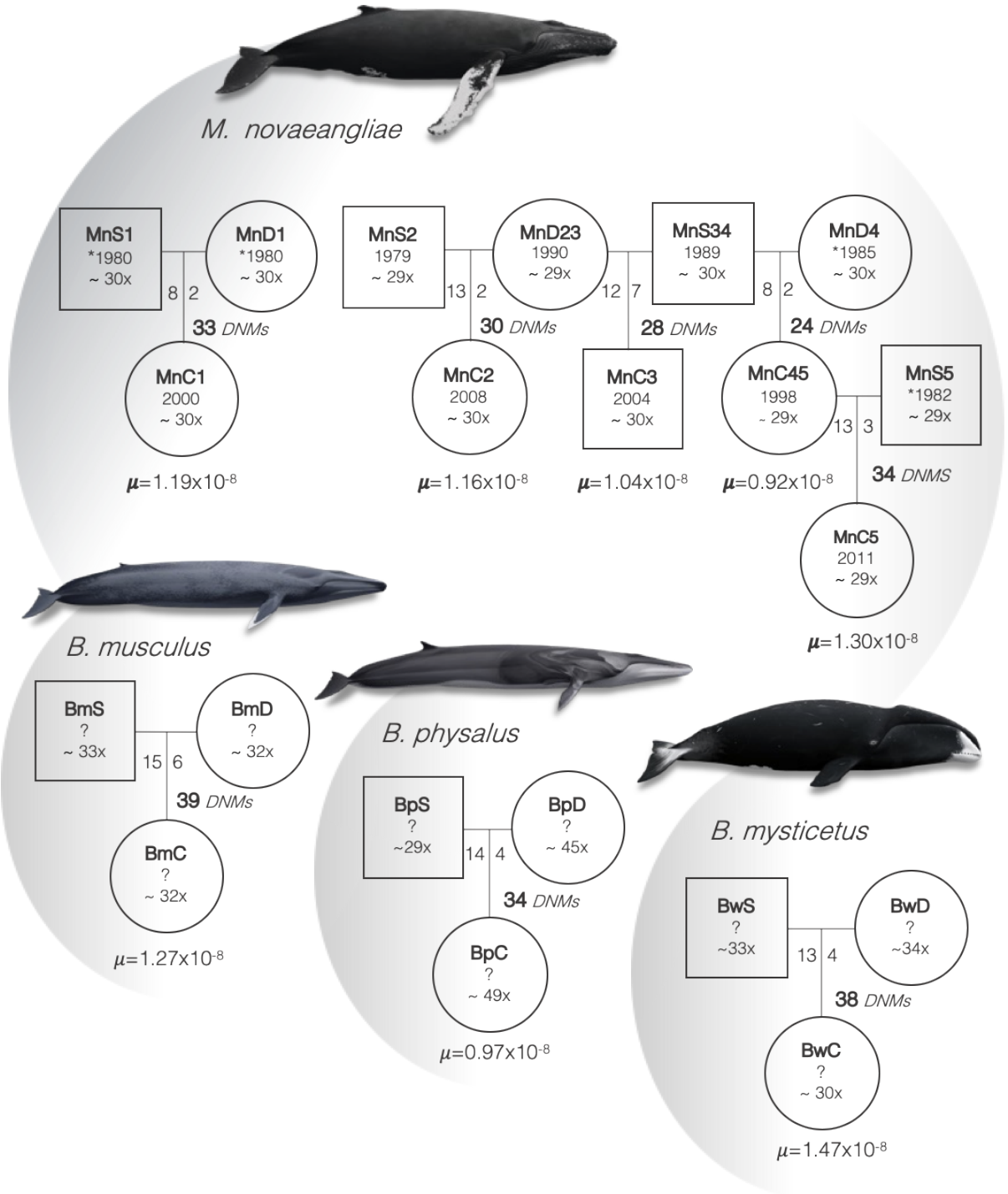

Fig. 1. Summary of the estimation of μ_{PED} in the nuclear genome per parent-offspring trio in humpback, blue, bowhead and fin whales. Squares and circles denote males and females, respectively, and contain sample identification number; birth year (or the year in which the

bioRxiv preprint doi: https://doi.org/10.1101/2022.10.06.510775; this version posted October 7, 2022. The copyright holder for this preprint (which was not certified by peer review) is the author/funder, who has granted bioRxiv a license to display the preprint in perpetuity. It is made available under aCC-BY-NC-ND 4.0 International license.

individual was first sighted, denoted by *), no previous sightings (denoted by ?) and mean genome sequence coverage. Along the vertical lines are listed; the total number of detected *DNMs* and the number of *DNMs* originating from the father (left) and the mother (right). μ_{PED}: the estimate obtained from the specific trio. Whale illustrations by Frédérique Lucas (size of whales is not to scale).

The complete genome was sequenced in all individuals to an average depth of ~30 and aligned against the blue whale genome (*15*). *DNMs* in the offspring genomes were identified by employing a modified version of Bergeron *et al.*'s (*16*) pipeline, manually curated and a subset of *DNMs* subsequently confirmed from Sanger sequencing. The accuracy of the modified pipeline and curation was assessed by reanalysing published data from macaques (*16*, *17*), which yielded a similar estimate of μ. A total of 260 *DNMs* were identified in the eight offspring, among which 126 were phased, and 76% were paternal (tables S2 & S3). The majority of *DNMs* consisted of transitions from a strong to a weak base with a most likely non-functional impact (fig. S6). All biallelic sites in the putative offspring were consistent with the presumed parents, i.e., segregating according to Mendelian expectations. This was also the case for *DNMs* transmitted across two generations in humpback whales (Fig. 1). Age data for the sires were scarce, but suggested a positive correlation between the number of paternal *DNMs* and paternal age at conception, in agreement with other studies (*16*, *18*, *19*). No *DNMs* were shared between half-siblings (Fig. 1) suggesting that most *DNMs* arose during meiosis.

DNMs were detected in 63% of the autosomal genome yielding estimates of μ_{PED} at 1.12×10^{-8} (range: $.93\times10^{-8}$-1.3×10^{-8}) and 1.17×10^{-8} (range: $.93\times10^{-8}$-1.47×10^{-8}) in both humpback whales alone and all baleen whales combined, respectively (Fig. 1, table S2). The latter estimate is very similar to estimates of μ_{PED} in humans and other large primates (Fig. 3, A) contrary to the notion of a lower μ in baleen whales. Prior acceptance of low μ_{PHY} estimates was mostly based on the hypothesized effects of a reduced metabolic rate in gigantic mammals (500× - 2,000× by weight relative to humans), resulting in lower levels of intracellular free radicals and consequently less DNA damage (*4*). It is possible, although somewhat implausible, that μ is lower in somatic cells compared to germline cells (*20*). However, in such a case, baleen whales would differ from other mammals in terms of a mechanism that solely lowers somatic, but not germline, mutation rates (e.g., DNA repair mechanisms). Barring such a unique mechanism, our findings do not provide sufficiently low rates of μ needed to explain Peto's Paradox, i.e., lower rates of cancer in gigantic mammals (*7*, *21*).

The hypervariable control region in the maternally transmitted mt genome is one of the most common genetic markers employed in population genetics towards a wide range of fundamental aspects in ecology and evolution. Contemporary levels of genetic diversity in baleen whales have been employed to infer unexpectedly high pre-exploitation abundances in North Atlantic baleen whales (*8*). These genetic assessments of the impacts of whaling were based on μ_{PHY}. The much smaller size of the mitochondrial genome (16.5KB), implies few, if any, *DNMs* in each offspring. Accordingly, a large sample of mother-offspring pairs (*22*) is necessary to obtain an estimate of μ_{PED} in the mt genome. We capitalized on the long-term research on North Atlantic humpback whales (*Megaptera novaeangliae*) in the Gulf of Maine since the 1970s. We identified 141 maternal lineages among 848 humpback whales, characterized by 20 different mt haplotypes, each numbering between two and 49 whales and spanning one to four generations. *DNMs* in the mt control region were evident as heteroplasmy and detected in the oldest known female in nine maternal lineages and at minimum one descendant to confirm germline heteroplasmy. In total, heteroplasmy was detected in five, three and one lineages at sites 82, 258 and 235 (table S5), respectively.

bioRxiv preprint doi: https://doi.org/10.1101/2022.10.06.510775; this version posted October 7, 2022. The copyright holder for this preprint (which was not certified by peer review) is the author/funder, who has granted bioRxiv a license to display the preprint in perpetuity. It is made available under aCC-BY-NC-ND 4.0 International license.

Heteroplasmy at site 82 was identified in three different mt haplotypes, confirming the presence of mutational hotspots (*23*). The *DNMs* detected as heteroplasmy in seven lineages, yielded mt control region haplotypes already present in the population (table S5), i.e., *DNMs* that may go unaccounted in estimates of μ_{PHY} (*9*).

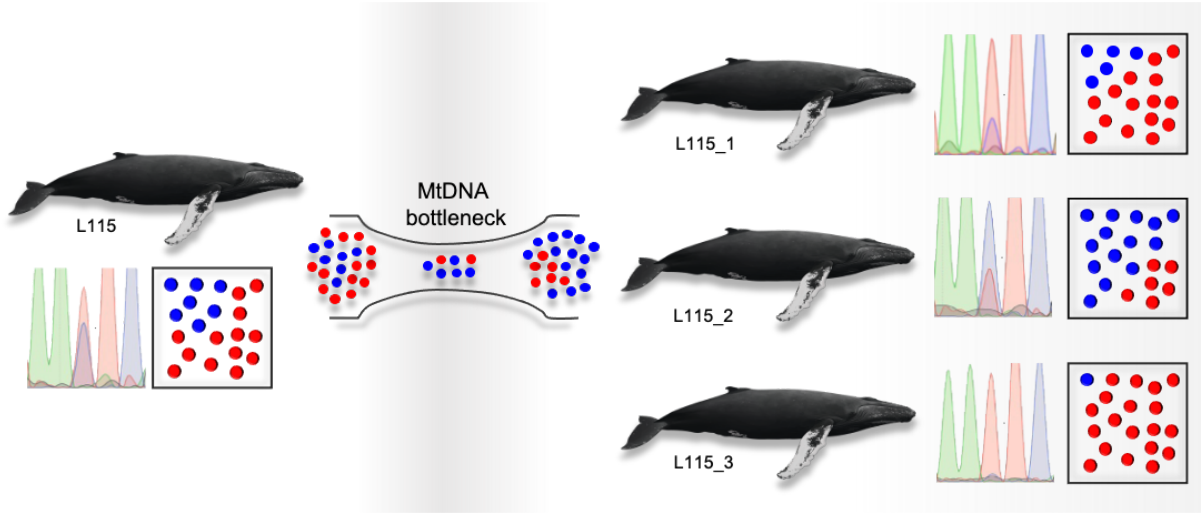

Fig. 2. An example of the change in mt haplotype frequencies of a point heteroplasmy after the transmission bottleneck during oocyte production in a humpback whale cow and her three calves as evident in Sanger sequencing chromatograms (left-hand side square) and sequence read frequencies (right-hand side square). The relative frequencies of the two mt haplotypes were reversed in calf 2 compared to the mother. In calf 3, the heteroplasmy was undetectable by Sanger sequencing but detected among the sequenced reads. Whale illustrations by Frédérique Lucas.

We inferred μ_{PED} from the generational change in the frequency of each variant at the heteroplasmic site as per Hendy and colleagues (fig. 2, *24*) from massive parallel sequence data with an average read depth at 6,900 (*20*). In total, 47 maternal transmissions of a germline mt heteroplasmy were used to infer a median estimate of the number of segregating units at 10.4 (interquartile range, *IQR* 5-28.9, fig. S7) during the oocyte bottleneck. The number of segregating units was similar to, but at the lower end, of the range of values reported in other species (*22*, *26–29*). The final estimate of μ_{PED} for the mt control region was at 4.3×10^{-6} (*IQR* 1.55×10^{-6}-8.85×10^{-6}, table S6), similar to comparable estimates of μ_{PED} for the same mt region in humans (3.8×10^{-6}; *IQR* 1.18×10^{-6}-1.16×10^{-5}, *27*).

We assessed the consequence of our findings on previous estimates of pre-exploitation abundance of North Atlantic humpback whales that were inferred from contemporary levels of genetic diversity (*8*, *9*, *30*). Insights into the pre-exploitation abundance of baleen whales are not only relevant to their current level of endangerment, but also provide fundamental insights into the overall state of the historic oceans and the biomass they supported prior to human overexploitation. Our re-analysis was conducted as in previous studies (*8*, *30*) except for using the value of μ_{PED} for the mt control regions estimated here. We estimated an effective female population size of 2,561 (*IQR* 1,245-7,128), which translated into an abundance of 20,494 humpback whales (*IQR* 9,964-57,030). This estimate corresponds to only 14% of the lowest μ_{PHY}-based estimate based on mt control region sequences (150,000, credited to *9*, by *30*). Notably, the abundance based on our estimate of μ_{PED}, is similar to

bioRxiv preprint doi: https://doi.org/10.1101/2022.10.06.510775; this version posted October 7, 2022. The copyright holder for this preprint (which was not certified by peer review) is the author/funder, who has granted bioRxiv a license to display the preprint in perpetuity. It is made available under aCC-BY-NC-ND 4.0 International license.

non-genetic estimates of pre-exploitation humpback whale abundance (17,151-22,647, *10*). Together these results suggest that estimates of pre-exploitation whale abundance based on μ_{PHY} are likely strongly upward biased. Consequently, the most recent estimate of abundance of North Atlantic humpback whales (10,752, *31*) may be closer to pre-exploitation levels than suggested by previous genetic assessments (*8*, *9*, *31,* Fig. 3, B), and the carrying capacity of the pre-exploitation oceans was possibly correspondingly lower. However, whale abundance estimated in this manner represents a temporal harmonic mean, and therefore necessarily reflects the actual abundance at a specific time period (*2*). Perhaps most importantly, our re-analysis demonstrated how sensitive this kind of inference is to changes in the underlying parameter values (*2*).

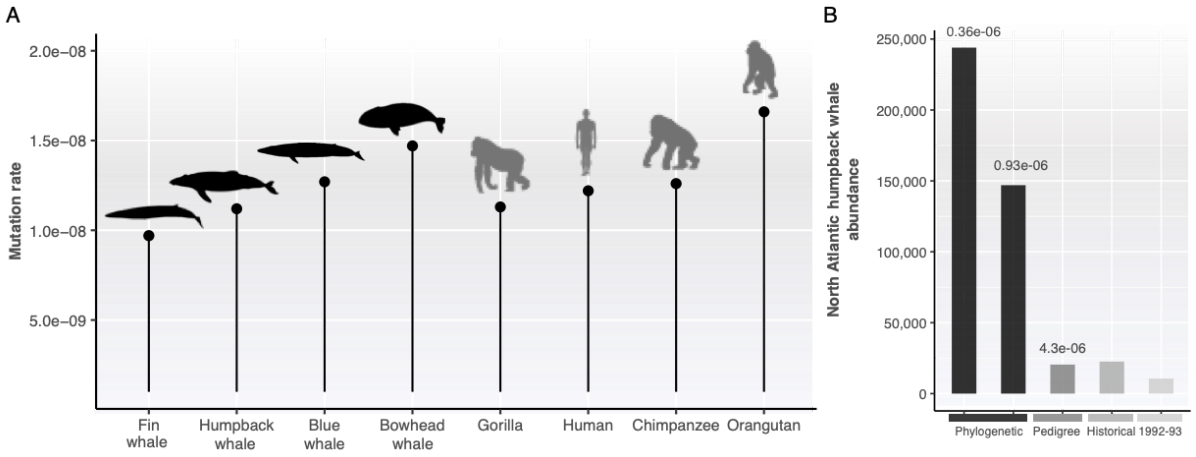

Fig. 3. A) Pedigree-based estimates of genome mutation rates for baleen whales (this study) and large primates (table S1, *18*, *32*). B) Estimates of contemporary and pre-exploitation abundance of North Atlantic humpback whales. Estimates based on μ_{PHY} were adjusted to match the generation time used in the original analysis and the annual rate of μ_{PHY} scaled to generations (18 years, *8*, *9*). Historical abundances estimated through non-genetic means (*10*). Most recent published abundance estimate (*31*).

The rate and nature of *DNMs* is at the center of evolution itself and in many ecological and evolutionary inferences. Differences in μ among taxonomic groups have fostered a wide array of intriguing hypotheses aimed at understanding their underlying causes (*1*). However, there are technical caveats in the estimation of μ_{PHY} that render comparisons difficult because the observed variation might reflect biological or analytical differences, as well as incomplete records. This study shows that direct, pedigree-based estimation of μ in natural populations of non-model species is entirely feasible without any prior knowledge, even in comparatively inaccessible large mammals with exceptionally wide ranges and long generation times. The results of the pedigree-based approach to directly estimate μ_{PED} in baleen whales have notable implications for studies of human impacts on the ecosystem and evolutionary cancer biology. Given the relative ease of detecting parent-offspring trios in large samples and the low costs of whole genome sequencing, we foresee a bright future in obtaining pedigree-based estimates of μ_{PED} across a wide range of biodiversity. The pedigree-based approach generates directly comparable data, which will facilitate novel insights across a range of fundamental and applied aspects. Pedigree-based detection of hundreds to thousands of *DNMs* will also provide new and more detailed insights into the nature and distribution of *DNMs* thereby improving evolutionary and population genetic inference methods in general.

bioRxiv preprint doi: https://doi.org/10.1101/2022.10.06.510775; this version posted October 7, 2022. The copyright holder for this preprint (which was not certified by peer review) is the author/funder, who has granted bioRxiv a license to display the preprint in perpetuity. It is made available under aCC-BY-NC-ND 4.0 International license.

Acknowledgements

We are indebted to the many staff who undertook the field and laboratory work over the years, and the long-term population research programs that made this work possible. We thank drs. Steve Beissinger and Oscar Gaggiotti for their valuable comments on this manuscript. The Center for Information Technology of the University of Groningen provided access and support to its Peregrine High Performance Computing cluster. We are grateful to Frédérique Lucas for providing whale drawings.

Funding

M.SM was supported by a doctorate fellowship from the University of Groningen. P.J.P and M.B acknowledge the support over the years by the University of Copenhagen, University of California Berkeley and Stockholm University. Additional funding was provided by the Aage V. Jensen Foundation (P.J.P), US National Marine Fisheries Service (P.J.P, M.B), the International Whaling Commission Scientific Committee (M.B., P.J.P), WWF-DK (P.J.P.), the Commission for Scientific Research in Greenland (P.J.P), the Greenland Home Rule (P.J.P), the European Union's Horizon 2020 Research and Innovation Programme under the Marie Skłodowska-Curie grant agreement no. 813383 (F.F., P.J.P.), and Consejo Nacional de Ciencia y Tecnología (V.RL.).

Author contributions

M.SM., M.B., V.RL, J.R., and P.J.P. conceived and designed the study. J.R., R.S., C.R., and M.H-J. provided samples and field data. M.B. and M.SM. conducted the laboratory work. M.SM., V.RL. and F.F. performed the bioinformatic and data analyses supervised by P.J.P. M.SM., M.B., and P.J.P interpreted the results with contributions from all authors. M.SM. and P.J.P, wrote the manuscript with input from all authors. All authors approved the final version.

Competing interests

The authors declare no competing interests.

bioRxiv preprint doi: https://doi.org/10.1101/2022.10.06.510775; this version posted October 7, 2022. The copyright holder for this preprint (which was not certified by peer review) is the author/funder, who has granted bioRxiv a license to display the preprint in perpetuity. It is made available under aCC-BY-NC-ND 4.0 International license.

Supplementary Materials

Materials and Methods

Samples

Skin biopsies were collected from free-ranging whales using a crossbow and modified arrows (*1*). The biopsies were stored in 6M NaCl with 25% dimethyl sulfoxide (*34*) at -80ºC before DNA extraction. Total cell DNA was extracted by standard phenol/chloroform extractions as described by Russel and Sambrook (*35*) or using QIAGEN DNEasy™ Blood and Tissue Kit (Qiagen Inc.) following the manufacturer's instructions. Extracted DNA was stored in 1xTE buffer (10 mM Tris–HCl, 1 mM EDTA, pH 8.0) at -20°C.

Nuclear mutation rate estimation

Paternity exclusion

Trios of whales were found by employing a paternity exclusion approach. Sex was determined by the differential amplification of the zinc finger coding regions, ZFX and ZFY(*36*) and by co-amplification of an SRY-specific region with one or more autosomal microsatellite loci (Bérubé, in prep). Samples were genotyped to up to 30-33 microsatellite markers (Bérubé, in prep). Every potential combination of a female with another whale was considered a putative mother-calf pair. These pairs were then compared with every male in the dataset. We sequenced the genome of all males that matched a mother-calf pair at every locus.

Genome sequencing

Whole-genome re-sequencing was carried out by the Beijing Genomic Institute. Pair-end (PE) sequencing, 100bp read-length, with free-PCR libraries, was performed on the BGISEQ500 platform for humpback, blue, and bowhead whale trios. Due to sample degradation, a modified protocol was employed for the bowhead whale samples in which DNA fragmentation was skipped. Fin whale samples were sequenced on a BGISEQ500 PE150 platform.

Genotype calling

The Bergeron et al. (*16*) pipeline was used to process the data and detect de novo mutations (*DNMs*) following the general guidelines described by Bergeron et al. (*17*). BWA-MEM (V0.7.17, *7*) was used to align the sequencing reads to the blue whale reference assembly (GCF_009873245.2, *8*) with the default options. PICARD (V2.25, *9*) was used to mark and remove duplicate reads. An initial set of variants was generated for recalibrating base quality scores. HaplotypeCaller and GenotypeGVCF were used to call variants. SNPs were filtered with GATK's (v4.1.8, *10*) recommended hard filtering thresholds (QD > 2.0, FS < 60.0, MQ > 40.0, MQRankSum > -12.5, ReadPosRankSum > -8.0, SOR < 3.0). The remaining SNPs were used as "known" variants by BaseRecalibrator to recalibrate quality scores on the initial set of aligned reads. After recalibrating the quality scores, variants were called again with HaplotypeCaller in BP_RESOLUTION mode. CombineGVCFs was used to merge gVCF files per autosomal chromosome and GenomicsDBImport, samples per trio. Joint genotyping of the combined gVCF files was performed with GenotypeGVCF and the same hard site filters were applied to the resulting VCFs. Kinship coefficients were calculated employing VCFtools (V0.1.16, *11*) with the --relatedness2 parameter employing all biallelic sites along the autosomal genome. In all trios, the kinship coefficient between the parents and the calf was >0.2 confirming the relatedness relation inferred from the microsatellite markers.

bioRxiv preprint doi: https://doi.org/10.1101/2022.10.06.510775; this version posted October 7, 2022. The copyright holder for this preprint (which was not certified by peer review) is the author/funder, who has granted bioRxiv a license to display the preprint in perpetuity. It is made available under aCC-BY-NC-ND 4.0 International license.

Identification of de novo mutations

Using GATK's VariantFiltration, mendelian violations were selected as potential *DNMs*. These are sites where the genotype of the offspring is not consistent with the genotypes of the parents based on Mendelian inheritance. Several filters were applied to the resulting mendelian violations to identify DNM candidates.

1. Both parents had to be homozygous for the reference allele with no reads assigned to the alternative allele (AD=0).
2. The number of reads for the alternative allele had to be between 30% and 70% of the total number of reads.
3. The read depth on each individual had to be between 0.5x-2x its average depth.
4. The genotype quality for a site had to be higher than 60 (GQ>60) on every individual of a trio.
5. At least one read of each strand had to support the alternative allele.

De novo mutation candidates that passed the previous filter were manually curated to detect false positives (fig. S4). Integrated Genomic Viewer was used to visualize realigned reads yielded by HaplotypeCaller. Candidate DNMs were considered false positives if the alternative allele on the offspring was supported just by reads on just one strand and there were multiple SNPs on the same reads not present in the parents. Although our pipeline resulted in a considerably higher number of putative *DNMs*, these were easy to identify and manually removed and it did not affect the performance of the pipeline (See Pipeline testing).

Phasing mutations

DNMs were phased by employing a read-based method described by Maretty et al. (*41*) This method employs reads that contain a *DNM* and at least another variable site that allows identifying the origin of the *DNM* if only one of the parents presents it.

Sanger sequencing DNMs

Primer-BLAST (*42*) was used to design primers to amplify and sequence a subset of *DNMs* detected in the blue whale trio and the humpback whale trio (table S4). The quality of the primers was further checked with AmplifX (v1.7, *14*). PCRs were carried out in 10 µl volumes; 1µl Taq Buffer (Tris-HCL 0.67M, $MgCl_2$ 0.02M, $(NH_4)_2SO_4$ 0.166M, β-mercaptoethanol 0.11M), 4µl dNTPs (2mM of each nucleotide), 1µl forward and reverse primers, 0.08µl Taq DNA polymerase, 1µl DNA template and 1.92µl of dubbed-distilled water. The PCR program was comprised of an initial denaturation at 92ºC for two minutes, followed by 35 cycles of 15 seconds at 95ºC, 15 seconds at 55ºC and 30 seconds at 72ºC. The program terminated with five minutes at 72ºC. Amplification products were checked by electrophoresis through 2% Agarose gels in 1X TBE buffer (Tris-borate-EDTA) at 175V for 30 minutes, followed by staining with ethidium bromide and visualization under fluorescent light. PCR products were cleaned with Shrimp Alkaline Phosphatase and Exonuclease I, as described by Werle et al. (*44*). Cycle sequencing of cleaned PCR products was undertaken using the primers mentioned above and the BigDye ® Terminator v3.1 Cycle Sequencing kit Applied Biosystems ™ Inc.) following the manufacturer's protocol. The cycle sequencing products were purified by ethanol sodium precipitation. The order of sequencing fragments was resolved by electrophoresis on an ABI 3730 DNA Analyzer TM (Applied Biosystems Inc.).

Gene annotation and putative functional effect

DNMs were annotated and classified using SNPEFF (v4.3, *16*) to check the gene position and primary functional impact effect. This software uses a reference database to annotate mutations according to their respective genomic position and allocate an impact category based on functional impacts, such as amino acid changes. First, the SNPEFF –build function was employed to create a local database using the blue whale reference assembly gene transfer format (GTF) annotation file as a reference

bioRxiv preprint doi: https://doi.org/10.1101/2022.10.06.510775; this version posted October 7, 2022. The copyright holder for this preprint (which was not certified by peer review) is the author/funder, who has granted bioRxiv a license to display the preprint in perpetuity. It is made available under aCC-BY-NC-ND 4.0 International license.

(NCBI accession number: GCF_009873245.2). VCFs containing *DNMs* were annotated and classified based on gene orthology using only canonical transcripts (-canon), and excluding downstream and upstream changes (-no-downstream -no-upstream). This filtering parameter avoids over-assignment of the putative impacts, leaving solely the most conservative putative impact effects. *DNMs* were then placed in one of each of the SNPEFF impact categories: *high* (e.g. loss of function mutations causing stop gain, stop loss, exon loss), *moderate* (e.g., missense with possible protein function disturbance, coding sequence mutations), *low* (non-detrimental for protein function, e.g, synonymous mutations), and *modifier* (non-impact variants, e.g, intergenic or intronic mutations). Any *DNM* presenting annotation warnings or errors were not considered and excluded from the analysis.

Estimating callable sites

To calculate the mutation rate per base pair, it was necessary to estimate the genome size in which *DNM* could be detected. For this step, the approach used by Bergeron et al was followed. Only sites where all individuals passed the following filters were considered; a) Hard site filters recommended by GATK (QD > 2.0, FS < 60.0, MQ > 40.0, MQRankSum > -12.5, ReadPosRankSum > -8.0, SOR < 3.0), b) both parents had to be homozygous to the reference allele with no reads assigned to the alternative alleles, c) read depth had to be 0.5x-2x the average read depth of the trio, d) the genotype quality scores had to be at least 60. A false-negative rate (FNR, α) due to the allelic balance filter was calculated; sites that were not called heterozygous on the calf despite both parents being homozygous for different alleles were counted and divided by the total amount of heterozygous sites. The mutation rate per generation was calculated employing the following equation (*16*); where m is the number of *DNM*, β the false positive rate (FPR), α the FNR and C the size of the callable genome.

$$\mu = \frac{m \times (1-\beta)}{(1-\alpha) \times 2 \times C}$$

Pipeline testing

Bergeron and colleagues (*17*) analysed a trio of rhesus macaques employing five different bioinformatic pipelines. The same trio was analysed with our pipeline. Employing exactly the same parameters we used for the whales resulted in a mutation rate (0.38×10^{-8} substitutions per site per generation) below what other groups obtained in Bergeron et al. (2022). This consisted of 18*DNMs* detected with no false positives and 88% of the genome covered. We consider that the parameters of a pipeline should be adjusted based on the type of data employed. Bergeron et al. (2022) employed a trio sequenced at a considerable higher sequencing depth (~60X). Thus, we found that with our pipeline and high coverage data the AD=0 filter is too stringent. Allowing AD≤2 resulted in similar results as other groups (0.46×10^{-8}-0.85×10^{-8}) with a mutation rate of 0.62×10^{-8}, 30 *DNMs* detected after manual curation (204 before), one false positive and 88% of the genome covered. As no false positives were detected by sequencing putative *DNMs*, the FPR obtained by analysing the macaque trio (β =0.033) was employed to estimate the mutation rates.

bioRxiv preprint doi: https://doi.org/10.1101/2022.10.06.510775; this version posted October 7, 2022. The copyright holder for this preprint (which was not certified by peer review) is the author/funder, who has granted bioRxiv a license to display the preprint in perpetuity. It is made available under aCC-BY-NC-ND 4.0 International license.

Mitochondrial mutation rate estimation

Sequencing

Samples were genotyped at 19 microsatellite markers; AC087 (*46*) EV001, EV037, EV094, EV096 (*47*), GATA028, GATA053, GATA098, GATA417, TAA031 (*48*) GATA97408 (Bérubé, in prep) GT011 (*49*), GT015, GT023, GT101, GT195, GT211, GT271, GT575 (*50*) following the protocol described in (*51*). The sequence of the first 500 base pairs (bp) at the 5' end of the mitochondrial control region was determined as described in Palsbøll et al. (*52*) using the primers BP16071R (*53*) and MT4F (*54*). Polymerase Chain Reaction (PCR, *25*) products were cleaned with Shrimp Alkaline Phosphatase and Exonuclease I, as described by Werle et al. (*44*). Cycle sequencing of cleaned PCR products was undertaken using the primers mentioned above and the BigDye ® Terminator v3.1 Cycle Sequencing kit Applied Biosystems ™ Inc.) following the manufacturer's protocol. The cycle sequencing products were purified by ethanol sodium precipitation. The order of sequencing fragments was resolved by electrophoresis on an ABI 3730 DNA Analyzer TM (Applied Biosystems Inc.).

Pedigree analysis

Through longitudinal studies, individual humpback whales were identified from their natural markings, including the pigmentation pattern of the ventral side of the fluke, the serrations along the trailing edge of the fluke and the shape and scarring of the dorsal fin (*56*). Mother-calf pairs were identified in the field based on their close, consistent association, stereotypical behaviors and size differential (*57*). Parentage analysis and pedigree estimation were carried out in the software FRANZ (*58*). The age at first possible reproduction was set at five years old for both sexes. The maximum number of candidates was set at 7,000 for fathers and 1,500 for mothers (Nmmax and Nfmax, respectively). Five chains were carried out for the simulated annealing with a maximum of 100,000,000 iterations. The Metropolis Hasting parameters consisted of ten chains with a burn-in of 2,000,000 followed by 40,000,000 and sampling every 200 iterations. FRANZ was run with different seeds ten times to estimate the consistency rate. Every maternal lineage present in the pedigree was extracted. A maternal lineage was defined as a founding mother -a mother without a known mother in the pedigree- and all her descendants through the maternal line.

Heteroplasmy discovery

PHFINDER (v1.0 *29*) was used to detect point heteroplasmy in the Sanger sequence electropherograms generated for samples in the maternal lineages. The first 500 bp of the mitochondrial control region of *M. novaeangliae*, started at position 15,490 and ended at 15,989 according to the mitogenome sequence NC_006927.1 (Genbank Reference Sequence, *30*). This sequence was used as reference for the alignment in PHFINDER. Heteroplasmies were sought in a 275bp segment that started at position 15,539 and ended at position 15,813 of the reference sequence. The heteroplasmy detection threshold was set at 15%, average base call quality 30, and secondary ratios 0.4. Lineages were removed when no electropherogram could be analyzed for the founding mother or in any individual in a first-generation. Whales for which no electropherogram could be analysed (low quality or incomplete sequence) were removed from the dataset. A detected heteroplasmy was considered to be present in the germ line and hence, transmittable to the offspring when the same heteroplasmy was detected in the founding mother and in at least one individual of the subsequent generations in the maternal line. For the purpose of this study, only maternal lineages in which a germ-line heteroplasmy was detected in the founding mother of a lineage were used for downstream analysis.

bioRxiv preprint doi: https://doi.org/10.1101/2022.10.06.510775; this version posted October 7, 2022. The copyright holder for this preprint (which was not certified by peer review) is the author/funder, who has granted bioRxiv a license to display the preprint in perpetuity. It is made available under aCC-BY-NC-ND 4.0 International license.

NGS sequencing

The mitochondrial genome was sequenced from skin samples of each individual in maternal lineages with a germ-line heteroplasmy to obtain a higher resolution of heteroplasmic frequencies. From several of these individuals, multiple skin samples were sequenced to estimate a measurement variance (see Bottleneck estimation). NGS library preparation was carried out following NEBNext Ultra II FS DNA Library Prep Kit for Illumina NEB #E7805) protocol, using NEBNext ® Multiplex Oligos for Illumina ® Dual Index Primers Set 1, NEB #7600). Default settings of the manufacturer's protocol were followed during library preparation. The starting material was 390ng of purified genomic DNA in a final volume of 26µl. The selected size for the fragmentation stage was 150bp-350bp. During the size selection of adaptor-ligated DNA, an insert size distribution of 150bp-250bp was selected as the final library size distribution of 270bp-350bp. Hybridization of the prepared libraries was carried out using myBaits® Mito kit Arbor Biosciences©) following the manufacturer's protocol. This kit uses biotinylated RNA "baits" complementary to sequences of the humpback whale mitogenome (Genbank NC_006927.1), enriching the mitochondrial DNA in the library. The hybridization incubation was carried out for 43 hours. After the non-targeted DNA was washed away, the libraries were amplified through PCR for 18 cycles following the manufacturer's protocol. The final dual-indexed library was diluted between 5-20 nM. Libraries sequencing was outsourced to The Hospital for Sick Children (Toronto, Canada) where paired-end Illumina next-generation sequencing (125bp) was carried out on the HiSeq2500 platform. Demultiplexing and adapter removal was performed at the sequencing site.

NGS data processing and heteroplasmy detection

The raw reads processing and calculation of minimum allele frequencies (MAF) for analysed heteroplasmies consisted of four stages.

Step 1 – Numt filtering

All raw reads were aligned with BOWTIE2 (v2.3.4.3, *31*) as "end to end" alignment employing the setting very_sensitive to the humpback whale nuclear assembly (Genbank GCA_004329385.1, *32*) supplemented with the mitochondrial control region (CR) with 250 extra base pairs at both ends to account for the mitogenome circularity (coordinates: 15234-16398, 1-250. Genbank NC_006927.1). SAMTOOLS (v1.9, *34*) was used to convert the resulting Sequence Alignment Map (SAM) file into a BAM file. After this, the BAM file was sorted and indexed (this process was repeated after each modification of a BAM file throughout the pipeline). From this BAM file, only paired reads that mapped in proper pair and primary alignment to the supplemented CR were kept for the downstream analysis. BEDTOOLS (v2.27.1, *35*) tool bamtofastq was used to convert the BAM file back into FASTQ format.

Step 2 – Consensus sequence

A consensus sequence was created for each sample. Reads obtained from Step 1 were realigned to the same CR (coordinates: 15234-16398, 1-250. Genbank NC_006927.1) with BOWTIE2 as "end to end" alignment employing the setting very_sensitive. SAMTOOLS was used to convert the resulting SAM file into a BAM file, removing some reads in the process (reads unmapped, mate unmapped, not primary alignments, reads failing platform, duplicates), retaining properly paired reads and filtering by a mapping quality of 20. Read groups were added to the BAM file using the PICARD (v2.18.5 , *9*) tool AddOrReplaceReadGroups. The HaplotypeCaller tool from GATK (v4.1 *10*) was used (default settings) to generate a Variant Call Format (VCF) file (*40*). The VCF file was used by GATK's tool FastaAlternateReferenceMaker to generate the consensus sequence of the sample. Finally, BLAST+ (v2.7.1) tool Dustmasker (*64*) was used to set in lowercase low complexity regions (i.e. regions containing simple sequence repeats) in the consensus FASTA sequence.

Step 3 – Alternative alleles read count

The second step generated a VCF file from which the MAF of potential heteroplasmies was obtained. For this, forward and reverse reads were aligned against the sample's consensus reference with BOWTIE2 (very sensitive settings). SAMTOOLS was used to convert the resulting SAM file into a BAM file as in Step 1. The tool MarkDuplicates from PICARD was used to remove PCR/optical

bioRxiv preprint doi: https://doi.org/10.1101/2022.10.06.510775; this version posted October 7, 2022. The copyright holder for this preprint (which was not certified by peer review) is the author/funder, who has granted bioRxiv a license to display the preprint in perpetuity. It is made available under aCC-BY-NC-ND 4.0 International license.

duplicates. A custom Python script was then used to filter from the SAM file reads that contained more than three mismatches; either INDELs or substitutions. After mismatch filtering, a second custom Python script was used to filter PCR/sequencing artefacts due to palindromic regions. For every read with mismatches, the script parsed the sequence of nucleotides from the mismatch position to the closest extreme of the read, either 5' or 3'. Then, using Biopython v1.73 (*65*) the reverse complement of the selected sequence was generated and aligned to its immediate region in the reference sequence. If every position aligned perfectly, the read was discarded. After this custom filtering, the SAM file was checked for errors with CleanSam from PICARD. The SAM file was then converted again to a BAM file. FixMateInformation from PICARD was used to verify mate-pair information between read mates. BCFTOOLS (v1.9, *38*) commands mpileup (filtering by mapping and per base quality; settings -q 30 -Q 30 -C 50) and call (settings: --ploidy 1 -A -m) were used to obtain a VCF file from which the number of reads assigned to each alternative allele were parsed.

Step 4 - Heteroplasmy detection

Each position's alleles were called based on the read counts extracted from the VCF files. The MAF was calculated as the percentage of reads that supported the second most common allele. For a position with multiple alleles to be considered heteroplasmic, we set a heteroplasmy detection limit similar to the one set by González et al. (*67*); MAF of 3% with read coverage depths of at least 500 and 1.5% MAF for depths of 3000x or more.

Bottleneck estimation

The effective size of the germ-line bottleneck that occurs during egg production was estimated following the model used by Millar et al. (*26*). This model is based on the assumption that when both variants of an heteroplasmy are neutral (i.e. under no selection), the inheritance will be based on a binomial distribution with parameters p, the mother's MAF, and N, the germ-line bottleneck size in segregating units. Thus, the actual variance in MAF between mother and calf (from now on, genetic variance, σ^2genetic) will be dependent on the aforementioned parameters as shown in equation (1).

$$\sigma^2 = \frac{p(1-P)}{N} \quad \text{(eqn1)}$$

Millar and colleagues estimated the genetic variance as the raw variance (σ^2raw) minus two times the heteroplasmy measurement variance (equation 3). In this equation, σ^2raw is the squared difference between the maternal and the calf MAFs (equation 2) and σ^2measure (measurement variance) is the uncertainty measuring the heteroplasmy proportions. The measurement variance is subtracted twice as two measurements are taken for each mother-calf pair.

$$\sigma^2_{raw} = (MAF_{mother} - MAF_{calf})^2 \quad \text{(eqn 2)}$$

$$\sigma^2_{genetic} = \sigma^2_{raw} - 2\sigma^2_{measure} \quad \text{(eqn 3)}$$

Transmission events where the MAF between mother and calf do not change would result in negative values of genetic variance when employing equation (3). To prevent this, we estimated the genetic variance by both adding and subtracting the measurement variance from every measurement (equation 4). This produced an upper and lower limit of the actual MAF value (Mu, Ml, maternal upper and lower MAF value respectively. Cu, Cl, calf upper and lower MAF value respectively). The measurement variance was calculated by obtaining the pooled variance from the MAFs from whales with a germ-line heteroplasmy in which more than one biopsy was sequenced (table S6). This accounted not only for technical uncertainties in the heteroplasmy measurement but also for other biological uncertainties, although with several limitations. A better approach to estimate the effects of non-germ-line bottlenecks in the measured heteroplasmy proportions would be to use samples from different tissues (i.e. skin and blood). This would not only take into account the effects of mitotic bottlenecks but also the developmental ones from embryonic tissue differentiation (*68*, *69*). Obtaining different tissues from live whales was not feasible, thus assuming that the obtained measurement variation due to mitotic bottlenecks equals the overall variation (germ-lime, developmental and

bioRxiv preprint doi: https://doi.org/10.1101/2022.10.06.510775; this version posted October 7, 2022. The copyright holder for this preprint (which was not certified by peer review) is the author/funder, who has granted bioRxiv a license to display the preprint in perpetuity. It is made available under aCC-BY-NC-ND 4.0 International license.

mitotic bottlenecks) was a necessary assumption. Several studies in other species (*69*, *70*) have shown that the effect of the germ-line bottleneck is far more significant in determining heteroplasmy proportions. The raw variance between mother and calf was calculated for all four possible value combinations. The genetic variance for the mother-calf pair was set as the average of the raw variances (equation 4).

$$\sigma^2_{genetic} = \frac{(MAF_{Mu} - MAF_{Cu})^2 + (MAF_{Mu} - MAF_{Cl})^2 + (MAF_{Ml} - MAF_{Cu})^2 + (MAF_{Ml} - MAF_{Cl})^2}{4}$$

(eqn 4)

Mutation rate estimation

The mitochondrial control region germ-line mutation rate (μ), was estimated as described by Hendy et al. (*71*) and Millar et al. (*26*). They defined mutation rate as "the rate at which a base substitution is incorporated into all mitochondrial genomes of an individual". Their model defines that new mutations, assuming neutrality and an equal probability to be transmitted, enter the germ line at rate α. Of these mutations, only 1/N are expected to go to fixation, meaning that μ=α/N. To be able to detect an heteroplasmy, the MAF has to be higher than a set threshold δ dependent on the detection method used. In this study, for Sanger sequencing chromatograms the detection limit was set to δ=0.15. The model assumes that given δ, most heteroplasmies are lost without being detected and most heteroplasmies that reach δ do not go to fixation. Thus, the proportion of sites with observed heteroplasmies (β) can be approximated as $\beta = 2\alpha\ln(1/\delta - 1)$. Being β the number of founding mothers with a detected germ-line heteroplasmy divided by the number of maternal lineages times the number of base pairs analysed. A simulation was used to correct the unequal number of whales and biopsies in heteroplasmic pedigrees. Only the first generation of each lineage was considered. For each simulation, one random sample from the founding mother and a sample from a random calf was chosen. Then it was checked whether using only those samples a germline heteroplasmy would have been detected. From 100 simulations, we obtained an average of 6 lineages in which germ line heteroplasmy would have been detected with equal sampling. Solving for α (μ=α/N) in $\beta = 2\alpha\ln(1/\delta - 1)$ one obtains equation (6) used to estimate the mutation rate per generation.

$$\mu = \frac{\beta}{2N_x \ln(\delta^{-1} - 1)}$$ (eqn 6)

Population size estimation

The resulting mutation rate was used to estimate the long-term effective population size of North Atlantic humpback whales as done by Roman and Palumbi (*72*). With the exception of the mutation rate, all parameters were kept the same for the purpose of comparison. We employed equation $\theta = Ne_f\mu$, being θ the genetic diversity of the population, Ne_f the effective population size of females and μ, our estimate of the mutation rate per generation. We used the estimates of θ=0.022 calculated in their study as the section of the control region used in both studies largely overlaps (210bp). Total census size was calculated employing a conversion factor of eight; Ne_f was converted to total Ne by multiplying by two, considering a 1:1 sex ratio (*73*). Ne was then converted to the total number of breeding adults employing a ratio of two (*74*). Finally, to account for juveniles we multiplied again by two (*72*, *75*).

bioRxiv preprint doi: https://doi.org/10.1101/2022.10.06.510775; this version posted October 7, 2022. The copyright holder for this preprint (which was not certified by peer review) is the author/funder, who has granted bioRxiv a license to display the preprint in perpetuity. It is made available under aCC-BY-NC-ND 4.0 International license.

Fig. S1. Changes in the mutation rate (top) and percentage of the callable genome (bottom) with different genotype quality (GQ) thresholds.

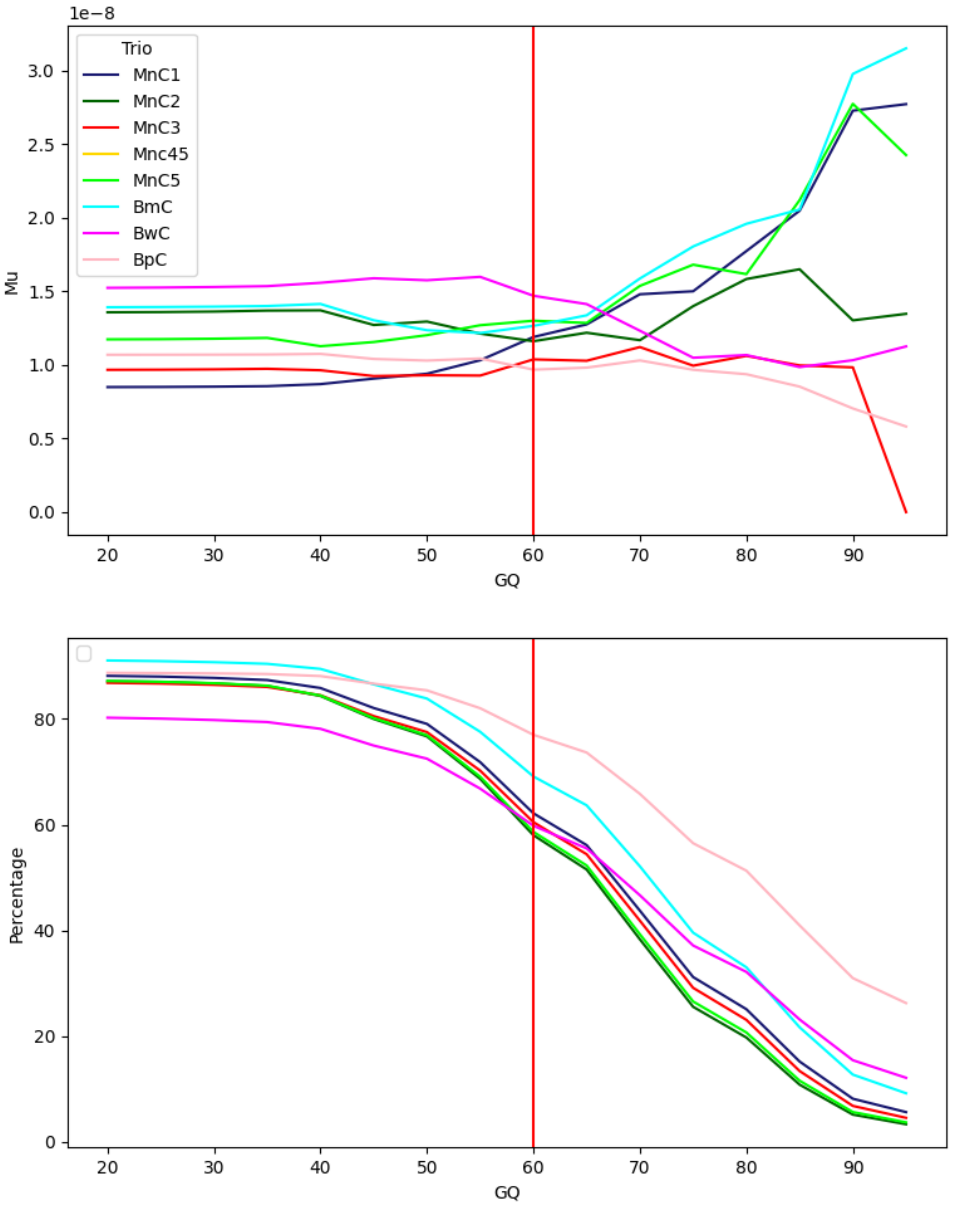

bioRxiv preprint doi: https://doi.org/10.1101/2022.10.06.510775; this version posted October 7, 2022. The copyright holder for this preprint (which was not certified by peer review) is the author/funder, who has granted bioRxiv a license to display the preprint in perpetuity. It is made available under aCC-BY-NC-ND 4.0 International license.

Fig. S2. Location of *DNMs* on all humpback whale trios along the chromosomes.

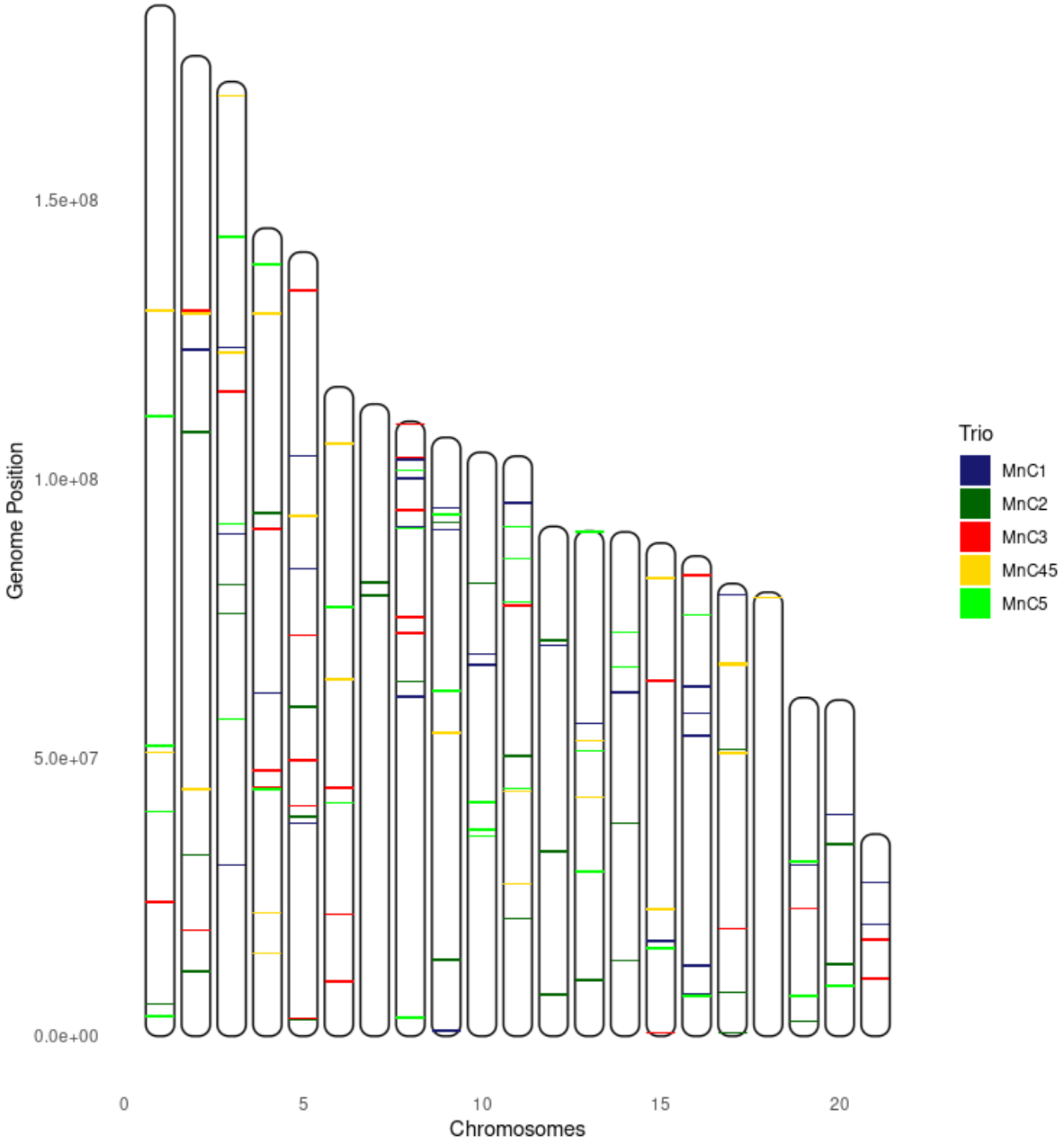

bioRxiv preprint doi: https://doi.org/10.1101/2022.10.06.510775; this version posted October 7, 2022. The copyright holder for this preprint (which was not certified by peer review) is the author/funder, who has granted bioRxiv a license to display the preprint in perpetuity. It is made available under aCC-BY-NC-ND 4.0 International license.

Fig. S3. Location of *DNMs* on the blue, fin and bowhead whale trios along the chromosomes.

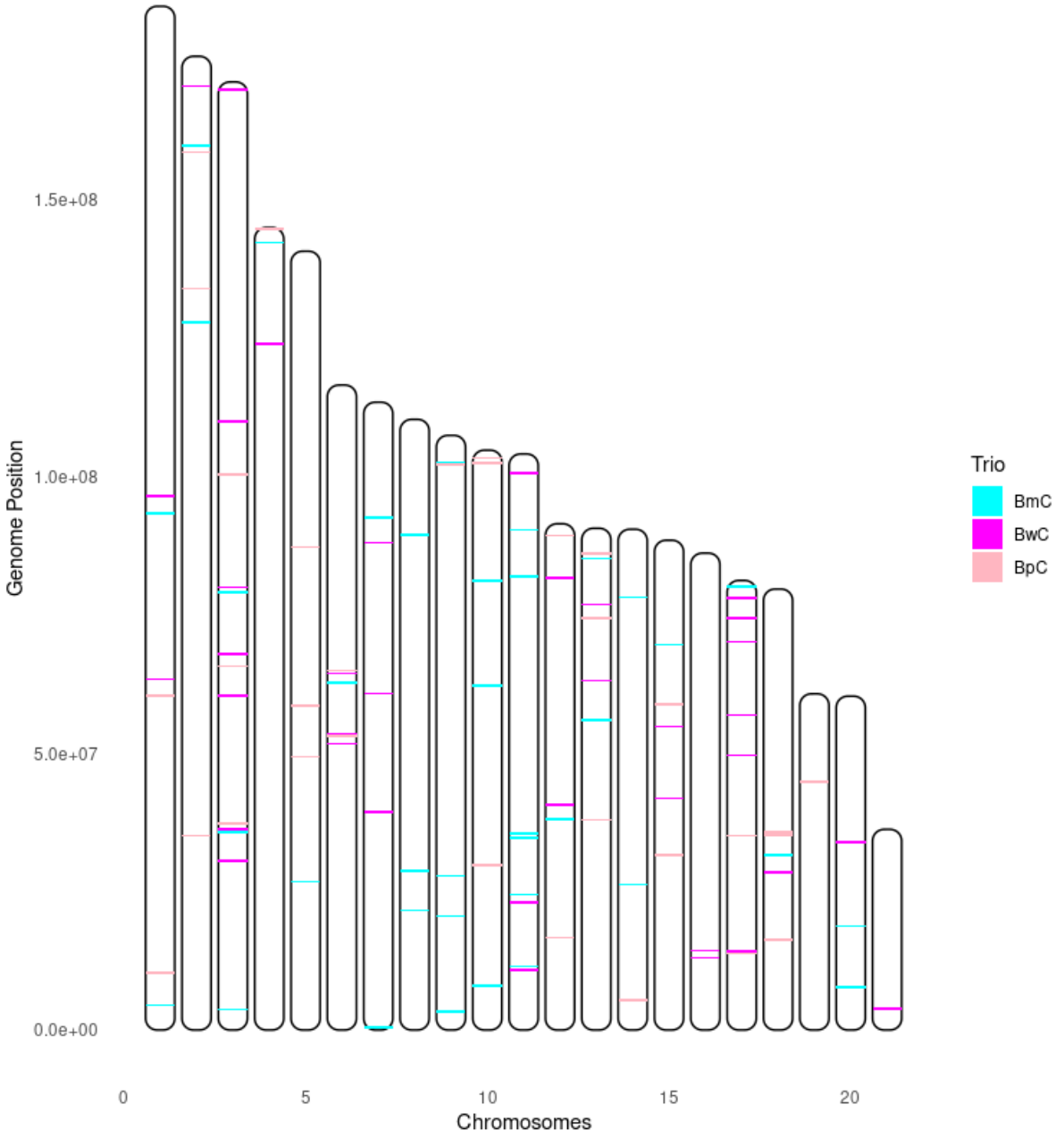

bioRxiv preprint doi: https://doi.org/10.1101/2022.10.06.510775; this version posted October 7, 2022. The copyright holder for this preprint (which was not certified by peer review) is the author/funder, who has granted bioRxiv a license to display the preprint in perpetuity. It is made available under aCC-BY-NC-ND 4.0 International license.

Fig. S4. Example of manual curation of *DNMs* on IGV viewer. Top image shows a putative *DNM* that passed curation. From top to bottom, calf, mother and father. Bottom image shows a putative *DNM* that did not pass manual curation.

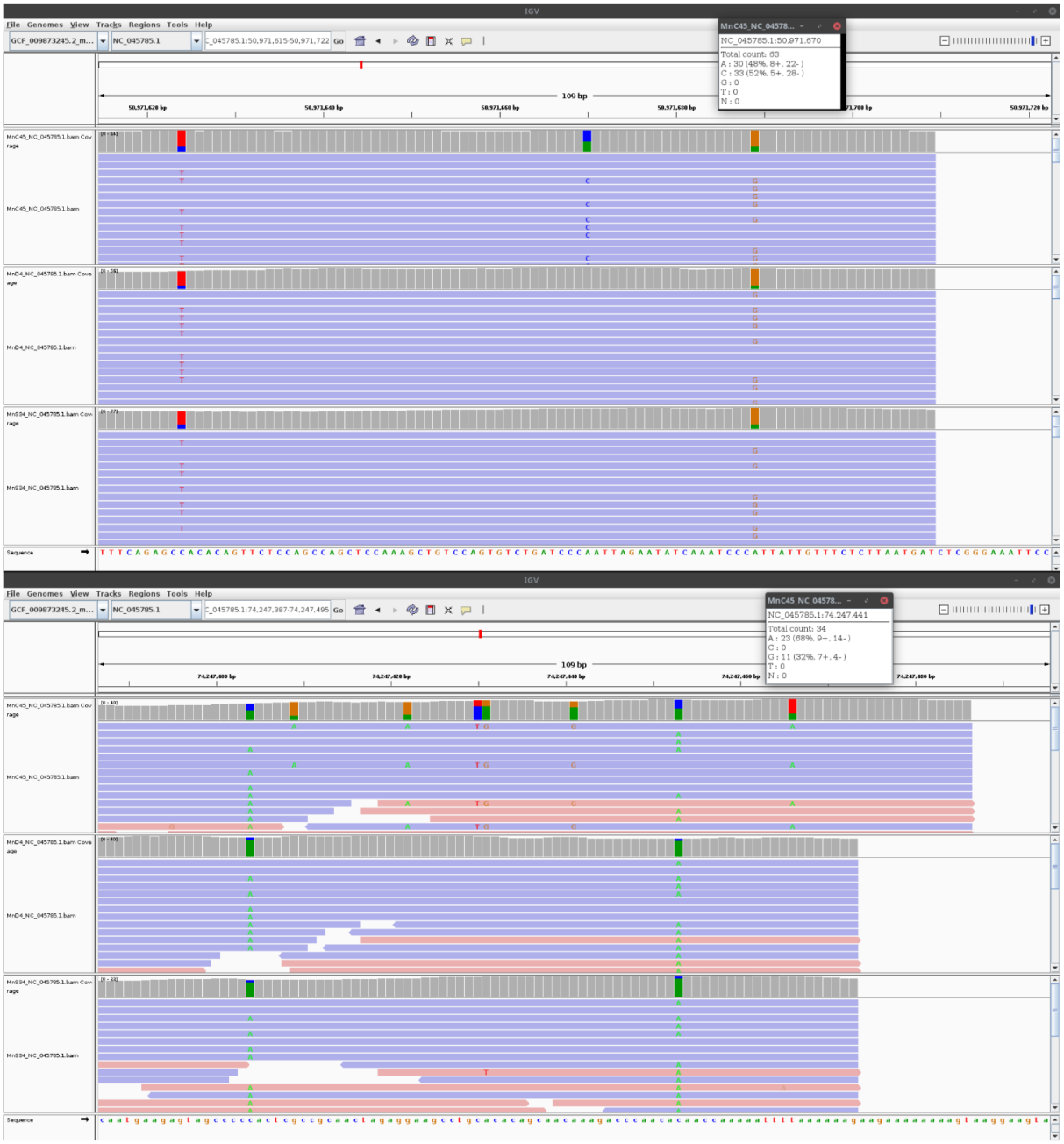

bioRxiv preprint doi: https://doi.org/10.1101/2022.10.06.510775; this version posted October 7, 2022. The copyright holder for this preprint (which was not certified by peer review) is the author/funder, who has granted bioRxiv a license to display the preprint in perpetuity. It is made available under aCC-BY-NC-ND 4.0 International license.

Fig. S5. Sanger sequencing chromatograms of 19 *DNM* that successfully amplified and sequenced. Blue rectangles indicate a *DNM* from the blue whale trio (BmC), in yellow humpback whale trio (MnC45). Top chromatogram, mother, middle calf, bottom father. *DNM* mutation in the middle position of each chromatogram

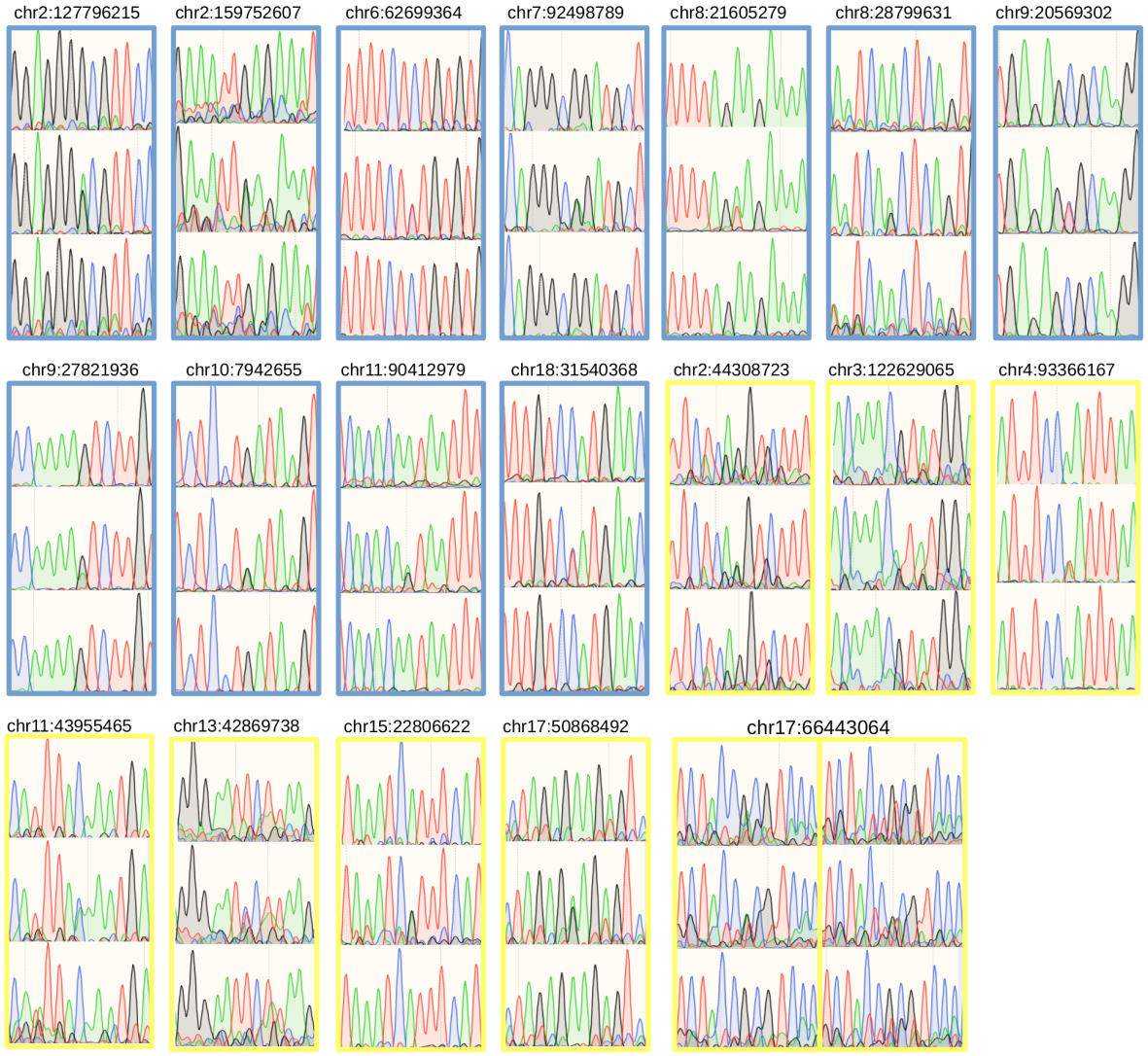

bioRxiv preprint doi: https://doi.org/10.1101/2022.10.06.510775; this version posted October 7, 2022. The copyright holder for this preprint (which was not certified by peer review) is the author/funder, who has granted bioRxiv a license to display the preprint in perpetuity. It is made available under aCC-BY-NC-ND 4.0 International license.

Fig. S6. Characterization of *DNM*. a) Type of *DNM*. b) Region and effect of *DNMs*.

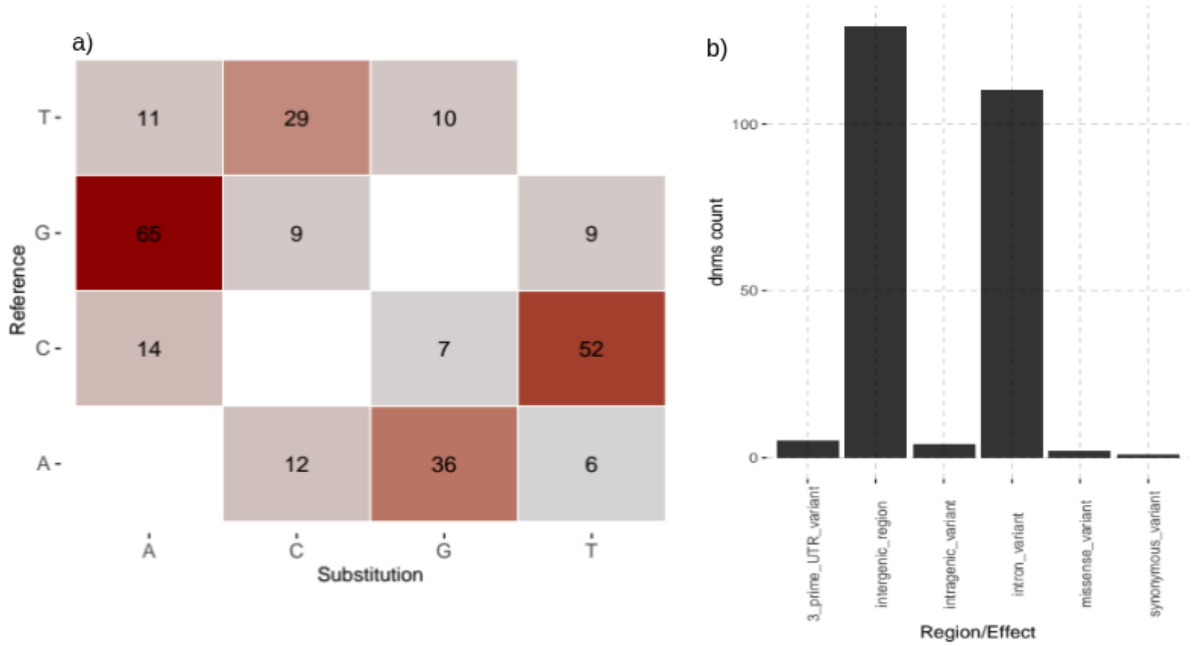

bioRxiv preprint doi: https://doi.org/10.1101/2022.10.06.510775; this version posted October 7, 2022. The copyright holder for this preprint (which was not certified by peer review) is the author/funder, who has granted bioRxiv a license to display the preprint in perpetuity. It is made available under aCC-BY-NC-ND 4.0 International license.

Fig. S7. Estimated number of segregating units (N) estimated from the change of heteroplasmic frequencies.

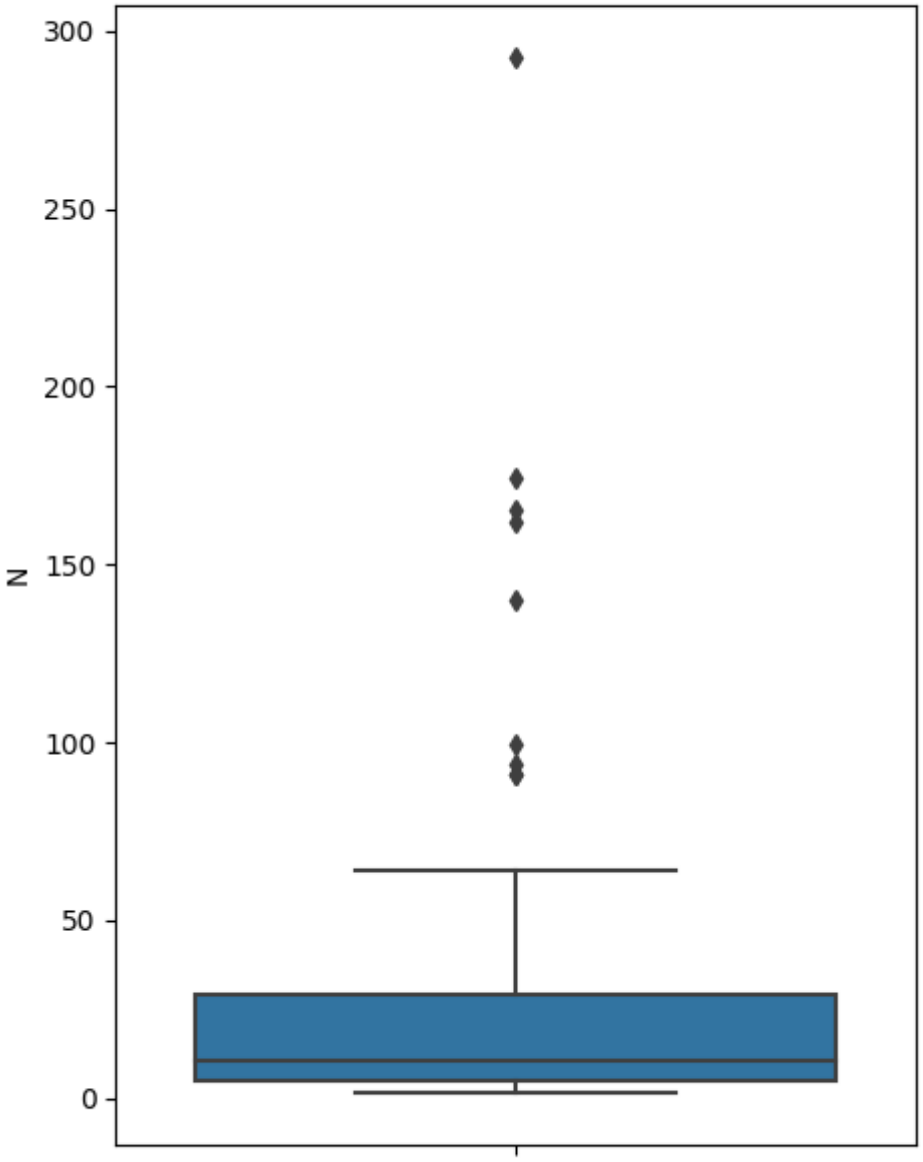

bioRxiv preprint doi: https://doi.org/10.1101/2022.10.06.510775; this version posted October 7, 2022. The copyright holder for this preprint (which was not certified by peer review) is the author/funder, who has granted bioRxiv a license to display the preprint in perpetuity. It is made available under aCC-BY-NC-ND 4.0 International license.

Table S1. Direct estimates of nuclear mutation rates on vertebrate species.

Species	Mu per generation	Reference
Herring (*Clupea harengus*)	0.2E-08	(*76*)
Cichlids (*Astatotilapia calliptera, Aulonocara stuartgranti,* and *Lethrinops lethrinus*)	0.35E-08	(*77*)
Pig (*Sus scrofa*)	0.36E-08	(*78*)
Mouse (*Mus musculus*)	0.39E-08	(*79*)
Marmoset (*Callithrix jacchus*)	0.43E-08	(*80*)
Gray wolf (*Canis lupus*)	0.45E-08	(*81*)
Collared flycatcher (*Ficedula albicollis*)	0.46E-08	(*13*)
Baboon (*Papio anubis*)	0.57E-08	(*82*)
Platypus (*Ornithorhynchus anatinus*)	0.7E-08	(*11*)
Rhesus macaque (Macaca mulatta)	0.77E-08	(*16*)
Owl monkey (*Aotus nancymaae*)	0.81E-08	(*83*)
Brown bear (*Ursus arctos horribilis*)	0.84E-08	(*84*)
Cat (*Felis catus*)	0.86E-08	(*85*)
Green monkey (*Chlorocebus sabaeus*)	0.94E-08	(*86*)
Gorilla (*Gorilla gorilla*)	1.13E-08	(*87*)
Cattle (*Bos Taurus*)	1.17E-08	(*88*)
Human (*Homo sapiens*)	1.22E-08	(*32*)
Chimpanzee (*Pan troglodytes*)	1.26E-08	(*87*)
Gray mouse lemur (*Microcebus murinus*)	1.52E-08	(*89*)
Orangutan (*Pongo abelii*)	1.66E-08	(*87*)

Table S2. Information about each trio: year calf was born, calf sex, age or minimum age of parents when calf was born, average depth of each trio after filters, number of *DNM* obtained with the pipeline and number of *DNM* that passed manual curation, phased mutation to each parent, number of bases of the autosomal genome that passed all filters, false negative rate and mutation rate.

Calf	Born	Sex	Mother	M Age	Father	F Age	Depth	Initial DNM	DNM	Phased	Maternal	Paternal	Callability	FNR	Rate
MnC1	2000	M	MnD1	>21	MnS1	>21	~30.2X	100	33	10	2	8	1387380708	0.033	1.19E-08
MnC2	2008	F	MnD23	18	MnS2	29	~29.1X	124	30	15	2	13	1294832914	0.036	1.16E-08
MnC3	2004	M	MnD23	14	MnS34	15	~29.8	103	28	19	7	12	1349925895	0.034	1.04E-08
MnC45	1998	F	MnD4	>13	MnS34	9	~29.5X	161	24	10	2	8	1308400548	0.04	9.24E-09
MnC5	2011	F	MnD45	13	MnS5	>30	~29.2X	111	34	16	3	13	1309027306	0.034	1.30E-08
BmC	NA	F	BmD	NA	BmS	NA	~32.2X	177	39	21	6	15	1546013551	0.037	1.27E-08
BwC	NA	F	BwD	NA	BwS	NA	~32.1X	376	38	17	4	13	1331220563	0.061	1.47E-08
BpC	2009	F	BpD	NA	BpS	NA	~41.2X	134	34	18	4	14	1719391485	0.012	9.68E-09

bioRxiv preprint doi: https://doi.org/10.1101/2022.10.06.510775; this version posted October 7, 2022. The copyright holder for this preprint (which was not certified by peer review) is the author/funder, who has granted bioRxiv a license to display the preprint in perpetuity. It is made available under aCC-BY-NC-ND 4.0 International license.

Table S3. List of positions of all *DNMs* and whether they were unphased (U), phased to the father (P) or to the mother (M). In bold *DNM* found in MnC45 that were transmitted to MnC5.

Calf	Chromosome	*DNMs*	Phase
MnC1	Chr2	123250494	U
MnC1	Chr3	30712312	P
MnC1	Chr3	90142215	U
MnC1	Chr3	123579014	U
MnC1	Chr4	61539962	U
MnC1	Chr5	38273433	P
MnC1	Chr5	83913722	U
MnC1	Chr5	104123224	P
MnC1	Chr8	60934463	U
MnC1	Chr8	91400989	U
MnC1	Chr8	100087168	P
MnC1	Chr8	103424558	U
MnC1	Chr9	955366	U
MnC1	Chr9	90922533	U
MnC1	Chr9	94805965	U
MnC1	Chr10	66614021	P
MnC1	Chr10	68624075	U
MnC1	Chr11	95663131	U
MnC1	Chr12	70155619	U
MnC1	Chr13	56170965	M
MnC1	Chr14	61639631	U
MnC1	Chr15	17035534	P
MnC1	Chr15	17071708	P
MnC1	Chr16	7560394	U
MnC1	Chr16	12720908	U
MnC1	Chr16	53960431	U
MnC1	Chr16	57914348	M
MnC1	Chr16	62677306	U
MnC1	Chr17	79175402	U
MnC1	Chr19	30665231	P
MnC1	Chr20	39797956	U
MnC1	Chr21	20104100	U
MnC1	Chr21	27560283	U
MnC2	Chr1	5749459	U
MnC2	Chr2	11560971	U
MnC2	Chr2	32464180	M

bioRxiv preprint doi: https://doi.org/10.1101/2022.10.06.510775; this version posted October 7, 2022. The copyright holder for this preprint (which was not certified by peer review) is the author/funder, who has granted bioRxiv a license to display the preprint in perpetuity. It is made available under aCC-BY-NC-ND 4.0 International license.

MnC2	Chr2	108458519	U
MnC2	Chr3	75839400	P
MnC2	Chr3	80997127	P
MnC2	Chr4	93900090	U
MnC2	Chr5	3032521	P
MnC2	Chr5	39415348	P
MnC2	Chr5	59095879	P
MnC2	Chr7	79068637	P
MnC2	Chr7	81447750	U
MnC2	Chr8	63626960	P
MnC2	Chr9	13673951	P
MnC2	Chr9	92153049	U
MnC2	Chr10	81317192	P
MnC2	Chr11	21100371	U
MnC2	Chr11	50308875	U
MnC2	Chr12	7522864	P
MnC2	Chr12	33131010	U
MnC2	Chr12	71075631	U
MnC2	Chr13	10116027	M
MnC2	Chr14	13556870	U
MnC2	Chr14	38202285	P
MnC2	Chr17	576379	U
MnC2	Chr17	7872693	U
MnC2	Chr17	51447384	P
MnC2	Chr19	2645963	U
MnC2	Chr20	12895998	P
MnC2	Chr20	34394901	U
MnC3	Chr1	24060116	P
MnC3	Chr2	19076584	U
MnC3	Chr2	130210842	U
MnC3	Chr3	115614823	U
MnC3	Chr4	44718329	P
MnC3	Chr4	47756745	P
MnC3	Chr4	91063666	P
MnC3	Chr5	3200933	P
MnC3	Chr5	41325633	M
MnC3	Chr5	49443178	M
MnC3	Chr5	71904681	M
MnC3	Chr5	133763983	P
MnC3	Chr6	9753815	U
MnC3	Chr6	21902221	P

bioRxiv preprint doi: https://doi.org/10.1101/2022.10.06.510775; this version posted October 7, 2022. The copyright holder for this preprint (which was not certified by peer review) is the author/funder, who has granted bioRxiv a license to display the preprint in perpetuity. It is made available under aCC-BY-NC-ND 4.0 International license.

MnC3	Chr6	44613027	P
MnC3	Chr8	72313906	U
MnC3	Chr8	75254610	P
MnC3	Chr8	94380212	M
MnC3	Chr8	103890829	M
MnC3	Chr8	109814839	U
MnC3	Chr11	77329600	P
MnC3	Chr15	661033	P
MnC3	Chr15	63816311	U
MnC3	Chr16	82780118	U
MnC3	Chr17	19228213	M
MnC3	Chr19	22937366	M
MnC3	Chr21	10326195	P
MnC3	Chr21	17327609	U
MnC45	**Chr1**	**50971670**	**P**
MnC45	Chr1	130183287	U
MnC45	Chr2	44308723	P
MnC45	**Chr2**	**129665965**	**U**
MnC45	Chr3	122629065	M
MnC45	Chr3	168759839	P
MnC45	Chr4	14824695	U
MnC45	Chr4	22179901	P
MnC45	Chr4	129644441	U
MnC45	Chr5	93366167	U
MnC45	**Chr6**	**64101747**	**P**
MnC45	**Chr6**	**106275881**	**U**
MnC45	**Chr9**	**54369065**	**U**
MnC45	**Chr9**	**93605498**	**U**
MnC45	Chr11	27329095	U
MnC45	Chr11	43955465	U
MnC45	Chr13	42869738	U
MnC45	Chr13	52987561	P
MnC45	Chr15	22806622	U
MnC45	**Chr15**	**82155882**	**P**
MnC45	Chr17	50868492	M
MnC45	Chr17	66443064	P
MnC45	Chr17	66889389	U
MnC45	**Chr18**	**78679788**	**U**
MnC5	Chr1	3552682	U
MnC5	Chr1	40316187	P
MnC5	Chr1	52132963	M

bioRxiv preprint doi: https://doi.org/10.1101/2022.10.06.510775; this version posted October 7, 2022. The copyright holder for this preprint (which was not certified by peer review) is the author/funder, who has granted bioRxiv a license to display the preprint in perpetuity. It is made available under aCC-BY-NC-ND 4.0 International license.

MnC5	Chr1	111233370	U
MnC5	Chr3	56853017	U
MnC5	Chr3	91961399	P
MnC5	Chr3	143473699	U
MnC5	Chr4	44253217	U
MnC5	Chr4	138520467	P
MnC5	Chr6	41870066	P
MnC5	Chr6	77006757	U
MnC5	Chr8	3332313	P
MnC5	Chr8	91119236	U
MnC5	Chr8	101568353	U
MnC5	Chr9	61887573	U
MnC5	Chr9	93567799	M
MnC5	Chr10	35869682	P
MnC5	Chr10	37099324	P
MnC5	Chr10	41933963	P
MnC5	Chr11	44491167	P
MnC5	Chr11	77856270	P
MnC5	Chr11	85717474	U
MnC5	Chr11	91355529	U
MnC5	Chr13	29542476	U
MnC5	Chr13	51216018	U
MnC5	Chr13	90469329	U
MnC5	Chr14	66225375	P
MnC5	Chr14	72490633	U
MnC5	Chr15	15711117	P
MnC5	Chr16	7183804	U
MnC5	Chr16	75635651	M
MnC5	Chr19	7274992	U
MnC5	Chr19	31372998	U
MnC5	Chr20	9062327	P
BmC	Chr1	4483519	P
BmC	Chr1	93286434	U
BmC	Chr2	127796215	U
BmC	Chr2	159752607	U
BmC	Chr3	3745675	P
BmC	Chr3	per785862	P
BmC	Chr3	79074147	P
BmC	Chr4	142304870	M
BmC	Chr5	26858356	P
BmC	Chr6	62699364	P

bioRxiv preprint doi: https://doi.org/10.1101/2022.10.06.510775; this version posted October 7, 2022. The copyright holder for this preprint (which was not certified by peer review) is the author/funder, who has granted bioRxiv a license to display the preprint in perpetuity. It is made available under aCC-BY-NC-ND 4.0 International license.

BmC	Chr7	416662	M
BmC	Chr7	92498789	U
BmC	Chr8	21605279	P
BmC	Chr8	28799631	U
BmC	Chr8	89517243	P
BmC	Chr9	3276241	U
BmC	Chr9	20569302	U
BmC	Chr9	27821936	M
BmC	Chr9	102425941	U
BmC	Chr10	7942655	U
BmC	Chr10	62157582	M
BmC	Chr10	81124648	U
BmC	Chr11	10958728	U
BmC	Chr11	11541947	U
BmC	Chr11	24513042	P
BmC	Chr11	34690236	M
BmC	Chr11	35486234	U
BmC	Chr11	81977232	U
BmC	Chr11	90412979	P
BmC	Chr12	38099499	M
BmC	Chr13	56038527	U
BmC	Chr13	85137147	P
BmC	Chr14	26290112	U
BmC	Chr14	78201420	P
BmC	Chr15	69637287	P
BmC	Chr17	80049486	P
BmC	Chr18	31540368	U
BmC	Chr20	7772222	U
BmC	Chr20	18796296	P
BpC	Chr1	10376411	P
BpC	Chr1	60377696	U
BpC	Chr2	35090542	U
BpC	Chr2	133891768	P
BpC	Chr2	158549327	M
BpC	Chr3	37295543	P
BpC	Chr3	65755303	P
BpC	Chr3	100324656	P
BpC	Chr4	144717008	P
BpC	Chr5	49324046	U
BpC	Chr5	58594696	U
BpC	Chr5	87237324	P

bioRxiv preprint doi: https://doi.org/10.1101/2022.10.06.510775; this version posted October 7, 2022. The copyright holder for this preprint (which was not certified by peer review) is the author/funder, who has granted bioRxiv a license to display the preprint in perpetuity. It is made available under aCC-BY-NC-ND 4.0 International license.

BpC	Chr6	53122206	P
BpC	Chr6	64951470	M
BpC	Chr6	64967041	M
BpC	Chr9	102170648	U
BpC	Chr10	29736182	U
BpC	Chr10	102497190	U
BpC	Chr10	103384078	M
BpC	Chr12	16694364	U
BpC	Chr12	89280044	U
BpC	Chr13	37929915	U
BpC	Chr13	74347019	P
BpC	Chr13	86102353	P
BpC	Chr14	5381311	U
BpC	Chr15	31624787	U
BpC	Chr15	58852704	U
BpC	Chr17	14032573	P
BpC	Chr17	35150861	P
BpC	Chr18	16273753	P
BpC	Chr18	35214863	U
BpC	Chr18	35720207	U
BpC	Chr18	35876726	U
BpC	Chr19	44874727	P
BwC	Chr1	63375732	U
BwC	Chr1	96507115	U
BwC	Chr2	170542042	P
BwC	Chr3	30506100	M
BwC	Chr3	36265009	P
BwC	Chr3	60419107	P
BwC	Chr3	67948875	U
BwC	Chr3	79975192	P
BwC	Chr3	109932469	U
BwC	Chr3	169811934	U
BwC	Chr4	124026351	P
BwC	Chr6	51708370	U
BwC	Chr6	53555190	U
BwC	Chr6	64458460	U
BwC	Chr7	39418501	U
BwC	Chr7	60745229	U
BwC	Chr7	88046196	M
BwC	Chr11	10763065	P
BwC	Chr11	10985568	P

bioRxiv preprint doi: https://doi.org/10.1101/2022.10.06.510775; this version posted October 7, 2022. The copyright holder for this preprint (which was not certified by peer review) is the author/funder, who has granted bioRxiv a license to display the preprint in perpetuity. It is made available under aCC-BY-NC-ND 4.0 International license.

BwC	Chr11	23000153	P
BwC	Chr11	100612370	P
BwC	Chr12	40697849	U
BwC	Chr12	81720861	P
BwC	Chr13	63132061	U
BwC	Chr13	76875822	U
BwC	Chr15	41791794	U
BwC	Chr15	54862159	M
BwC	Chr16	13039351	P
BwC	Chr16	14298429	U
BwC	Chr17	14264147	U
BwC	Chr17	49666977	M
BwC	Chr17	56858682	P
BwC	Chr17	70169596	U
BwC	Chr17	74382084	U
BwC	Chr17	78102952	U
BwC	Chr18	28474071	P
BwC	Chr20	33963838	U
BwC	Chr21	3833003	U

Table S4. Primers designed for PCR validation of *DNMs*. TM, annealing temperature. PCR, whether all samples werere amplified correctly and specifically. Seq, whether Sanger sequencing produced clean chromatograms. FP, false positive.

Calf	Chrom	Postion	Forward (5'-3')	Reverse (5'-3')	TM	PCR	Seq	FP
BmC	1	4483519	GCTTTTGCGCAGGATGGTAG	GCTGGTGGAAAAGATCGTGT	56-55	No	-	-
BmC	1	93286434	CCTGTGTGTTGTGCTCTAGGA	CAGCTAGCCTGATATAATTGTGGA	56-54	Yes	No	-
BmC	2	127796215	CTGTGACTGGCAATCTGAAGGA	GGAAGTTGGGCTAGGTGTTGT	56-56	Yes	Yes	No
BmC	2	159752607	GGCATTGTAGAGAATGATGACTGA	CAGGGATTGTTTGGCACAGAC	54-56	Yes	Yes	No
BmC	4	142304870	CCCAGTGTACCGTCCTTAGA	ATTCTCACACGTGCTTTGTGTC	54-56	No	-	-
BmC	5	26858356	TCCAGGAGAGACTGAAAACAGC	CTGTGATAGATGAGTCCGTGAAC	56-54	Yes	No	-
BmC	6	62699364	GATCTTGACTCCCTTCCAGGAAC	TGGTTCCACACATCTGGCTA	56-55	Yes	Yes	No
BmC	7	92498789	TTCACAGATGCGGAAATGGTC	GCAGTCCACTCCAGACCTATC	55-56	Yes	Yes	No
BmC	8	21605279	GGTTCTACTGGAATGCTGTCA	AGTGTCCATTGAAGCACAGAA	54-54	Yes	Yes	No
BmC	8	28799631	GTGGTGAGCAAACAGTAATCTGTG	CAACAGATAGAGTTTCCCTTGTGTG	56-55	Yes	Yes	No
BmC	8	89517243	CTGACCCAAACCAATAACATATGCC	GTGAATGAAATGGAGGCATCTGG	56-56	No	-	-
BmC	9	20569302	ACCCATTCCAGTCCAACCTAAG	AGTCACTGATCTGGTTCAAGGTT	55-55	Yes	Yes	No
BmC	9	27821936	AATCTGGGTGTCCAAAATGCT	GAGTGCAGTAGGGCATTATGTT	54-54	Yes	Yes	No
BmC	10	7942655	GGAGAATGGATATGTATTTCAGAAGGGA	CTTGCTGTGAGACCTTCCACT	56-56	Yes	Yes	No
BmC	10	81124648	GCTCCCTTGGTGGCTAATGT	GTAAAGTGAGGTGCCCCAGAT	56-56	Yes	No	No
BmC	11	11541947	CCAAGTGCTGTCAAGTCATGC	ACGAATGCATAAGGGACAAGG	56-54	Yes	No	No
BmC	11	90412979	TTTCCTAGCAAGGTAGCTGTGT	GAACCGAGGTGCAAAATAAGCC	55-56	Yes	Yes	No
BmC	18	31540368	TGTAACACGCATGTTTTCAGGA	CTCTTCACTTGCCTAGATTTGTCA	55-54	Yes	Yes	No
MnC45	1	130183287	TGCTTGGCACCATTCAAGTTCAGG	GAAGCTACACAACCAGCCATCCT	60-58	No	-	-
MnC45	2	44308723	ACTTAGTTAGCTTAGCGGTCATCT	CGGAAAATTCCACTCACAGAGC	55-56	Yes	Yes	No

MnC45	3	122629065	TGTAGCTGTGTCAGAGGGTGTA	CCCCATAAATTCCTGGTTCTTTCT	56-54	Yes	Yes	No
MnC45	5	93366167	TGAAGAGGGTGAATCCCTTGGTT	AGTTTGCAAGCATCTTCAATGTG	57-55	Yes	Yes	No
MnC45	11	43955465	GGTCTTTGCTCTCTGTAGCTCAT	TACTCGTCTGTTTCTCTTCTTCCA	56-55	Yes	Yes	No
MnC45	13	42869738	TGTCTACTCGGGGAACCTCA	AACTGGAATGACCAAATTGTGC	56-54	Yes	Yes	No
MnC45	15	22806622	GCCCTTGGTAAAGACTCAGTGAA	TGCTTTGCTCGTAAGCTCTGA	56-56	Yes	Yes	No
MnC45	17	50868492	GATTGTAGTGATGGGGAATTGGG	GTCACCTGATGCACAACTTGG	55-56	Yes	Yes	No
MnC45	17	66443064	CTGTGAAGCAGATGTGAATGGC	GACCTGCAGATTGATAGATGGAG	56-54	Yes	Yes	No

bioRxiv preprint doi: https://doi.org/10.1101/2022.10.06.510775; this version posted October 7, 2022. The copyright holder for this preprint (which was not certified by peer review) is the author/funder, who has granted bioRxiv a license to display the preprint in perpetuity. It is made available under aCC-BY-NC-ND 4.0 International license.

Table S5. Heteroplasmic lineages detected, number of individuals, generations and main and secondary haplotypes (based on the most supported haplotype present the founding mother).

Lineage	Position HP	Individuals	Generations	Main	Secondary
L11	258	6	2	HapH	HapC
L14	82	16	3	HapC	Novel
L47	258	3	2	HapC	HapH
L67	235	4	2	HapB	Novel
L76	82	7	3	HapN	HapG
L97	82	3	2	HapB	HapT
L105	258	9	3	HapH	HapC
L115	82	4	2	HapT	HapB
L127	82	5	2	HapN	HapG

Table S6. Heteroplasmy frequencies: position, mother, bases, number of reads assigned to each allele, heteroplasmic ratio, number of segregation units estimated (N) and estimated mutation rate.

Position	Mother	HP	Highest	Lowest	Ratio	Calf	HP	Highest	Lowest	Ratio	N	Mu
82	L127	T/C	5214	1926	27	L127_1	T/C	2913	625	17.7	21	2.13E-06
82	L127	T/C	5214	1926	27	L127_2	T/C	3099	483	13.5	10	4.29E-06
82	L127	T/C	5214	1926	27	L127_4	C/T	624	523	45.6*	3	1.72E-05
258	L47	G/A	2850	1611	36.1	L47_1	G/A	841	530	38.7	162	2.76E-07
258	L47	G/A	2850	1611	36.1	L47_2	G/A	4925	896	15.4	5	8.43E-06
235	L67	A/G	8657	3119	26.5	L67_1	A/G	1774	263	12.9	10	4.41E-06
235	L67	A/G	8657	3119	26.5	L67_2	A/G	5719	504	8.1	6	7.92E-06
235	L67	A/G	8657	3119	26.5	L67_3	A/G	6667	750	10.1	7	6.33E-06
82	L76	T/C	8686	2404	21.7	L76_5	T/C	6145	8	0	4	1.14E-05
82	L76	T/C	8686	2404	21.7	L76_1	T/C	1264	721	36.3	8	5.79E-06
82	L76	T/C	8686	2404	21.7	L76_2	T/C	8119	526	6.1	7	6.59E-06

82	L76	T/C	8686	2404	21.7	L76_4	T/C	4933	328	6.2	7	6.50E-06
82	L76	T/C	8686	2404	21.7	L76_3	T/C	1949	644	24.8	99	4.49E-07
82	L76_2	T/C	8119	526	6.1	L76_2.1	T/C	2609	204	7.3	64	6.96E-07
337	L97	C/T	3426	1713	33.3	L97_1	T/C	3616	2439	40.3*	3	1.41E-05
337	L97	C/T	3426	1713	33.3	L97_2	C/T	6654	3278	33	293	1.52E-07
258	L11	A/G	2175	1431	39.7	L11_1	G/A	5839	2173	27.1*	2	2.07E-05
258	L11	A/G	2175	1431	39.7	L11_2	A/G	1935	1413	42.2	174	2.56E-07
258	L11	A/G	2175	1431	39.7	L11_3	G/A	4900	2898	37.1*	4	1.02E-05
258	L11	A/G	2175	1431	39.7	L11_4	G/A	4804	2610	35.2*	4	1.19E-05
258	L11	A/G	2175	1431	39.7	L11_5	A/G	1996	495	19.8	6	7.52E-06
82	L14	C/T	466	52	10	L14_6	C/T	2275	577	20.2	8	5.53E-06
82	L14	C/T	466	52	10	L14_7	C/T	4032	174	4.1	21	2.10E-06
82	L14	C/T	466	52	10	L14_2	C/T	4656	769	14.2	36	1.25E-06
82	L14	C/T	466	52	10	L14_3	C/T	3027	141	4.5	24	1.87E-06

82	L14	C/T	466	52	10	L14_4	C/T	5720	2724	32.3	2	2.50E-05
82	L14	C/T	466	52	10	L14_5	C/T	703	3	0	10	4.28E-06
82	L14	C/T	466	52	10	L14_1	C/T	11774	16	0	10	4.28E-06
82	L14_6	C/T	2275	577	20.2	L14_6.1	C/T	5276	19	0	4	1.04E-05
82	L14_6	C/T	2275	577	20.2	L14_6.7	C/T	2468	12	0	4	1.04E-05
82	L14_6	C/T	2275	577	20.2	L14_6.3	C/T	5025	115	18.2	140	3.18E-07
82	L14_6	C/T	2275	577	20.2	L14_6.4	C/T	6041	1239	17	91	4.91E-07
82	L14_6	C/T	2275	577	20.2	L14_6.8	C/T	1824	66	3.5	6	7.92E-06
82	L14_6	C/T	2275	577	20.2	L14_6.6	C/T	3215	1999	38.3	5	9.27E-06
82	L14_6	C/T	2275	577	20.2	L14_6.2	C/T	3755	449	10.7	16	2.70E-06
82	L14_6	C/T	2275	577	20.2	L14_6.5	C/T	5173	1435	21.7	165	2.70E-07
258	L105	A/G	6007	3261	35.2	L105_3	A/G	2354	1057	31	91	4.91E-07
258	L105	A/G	6007	3261	35.2	L105_1	A/G	5856	2118	26.6	28	1.59E-06
258	L105	A/G	6007	3261	35.2	L105_2	A/G	9755	4413	31.1	94	4.75E-07

258	L105	A/G	6007	3261	35.2	L105_4	A/G	3319	2670	44.6	24	1.87E-06
258	L105_1	A/G	5856	2118	26.6	L105_1.1	A/G	7338	3996	35.2	24	1.86E-06
258	L105_1	A/G	5856	2118	26.6	L105_1.2	A/G	3877	2354	37.8	15	3.04E-06
258	L105_1	A/G	5856	2118	26.6	L105_1.3	A/G	5125	463	8.3	6	7.82E-06
258	L105_1	A/G	5856	2118	26.6	L105_1.4	A/G	2742	1465	34.8	26	1.71E-06
82	L115	T/C	5240	2643	33.5	L115_2	C/T	3728	1472	28.3	2	2.94E-05
82	L115	T/C	5240	2643	33.5	L115_3	T/C	12615	463	3.5	2	1.82E-05
82	L115	T/C	5240	2643	33.5	L115_1	T/C	1006	340	25.3	30	1.50E-06

*Transmission in which the allele supported by the highest number of reads flipped to the alternate allele in the calf.

bioRxiv preprint doi: https://doi.org/10.1101/2022.10.06.510775; this version posted October 7, 2022. The copyright holder for this preprint (which was not certified by peer review) is the author/funder, who has granted bioRxiv a license to display the preprint in perpetuity. It is made available under aCC-BY-NC-ND 4.0 International license.

Table S7. Heteroplasmy frequencies estimated for multiple biopsies of three individuals and the inferred pooled measurement error of the estimations.

Individual	Sample	Ratio
L105_1	MN0976	28.3
L105_1	MN0977	22.7
L105_1	MN0978	26.6
L105	MN0974	36.7
L105	MN0975	34.7
L105	MN1126	35.2
L76	MN0802	21.7
L76	MN0803	22.1
Pooled measurement error		0.019

bioRxiv preprint doi: https://doi.org/10.1101/2022.10.06.510775; this version posted October 7, 2022. The copyright holder for this preprint (which was not certified by peer review) is the author/funder, who has granted bioRxiv a license to display the preprint in perpetuity. It is made available under aCC-BY-NC-ND 4.0 International license.

References

1. L. Bromham, The genome as a life-history character: why rate of molecular evolution varies between mammal species. *Philos. Trans. R. Soc. B Biol. Sci.* **366**, 2503–2513 (2011).
2. P. J. Palsbøll, M. Zachariah Peery, M. T. Olsen, S. R. Beissinger, M. Bérubé, Inferring recent historic abundance from current genetic diversity. *Mol. Ecol.* **22**, 22–40 (2013).
3. A. P. Martin, S. R. Palumbi, Body size, metabolic rate, generation time, and the molecular clock. *Proc. Natl. Acad. Sci.* **90**, 4087–4091 (1993).
4. J. A. Jackson, C. S. Baker, M. Vant, D. J. Steel, L. Medrano-González, S. R. Palumbi, Big and Slow: Phylogenetic Estimates of Molecular Evolution in Baleen Whales (Suborder Mysticeti). *Mol. Biol. Evol.* **26**, 2427–2440 (2009).
5. R. Peto, F. J. Roe, P. N. Lee, L. Levy, J. Clack, Cancer and ageing in mice and men. *Br. J. Cancer*. **32**, 411–426 (1975).
6. A. M. Leroi, V. Koufopanou, A. Burt, Cancer selection. *Nat. Rev. Cancer*. **3**, 226–231 (2003).
7. M. Tollis, J. Robbins, A. E. Webb, L. F. K. Kuderna, A. F. Caulin, J. D. Garcia, M. Bérubé, N. Pourmand, T. Marques-Bonet, M. J. O'Connell, P. J. Palsbøll, C. C. Maley, Return to the Sea, Get Huge, Beat Cancer: An Analysis of Cetacean Genomes Including an Assembly for the Humpback Whale (*Megaptera novaeangliae*). *Mol. Biol. Evol.* **36**, 1746–1763 (2019).
8. J. Roman, S. R. Palumbi, Whales Before Whaling in the North Atlantic. *Science*. **301**, 508–510 (2003).
9. S. E. Alter, S. R. Palumbi, Comparing evolutionary patterns and variability in the mitochondrial control region and cytochrome b in three species of baleen whales. *J. Mol. Evol.* **68**, 97–111 (2009).
10. A. E. Punt, N. A. Friday, T. D. Smith, Reconciling data on the trends and abundance of North Atlantic humpback whales within a population modelling framework. *J. Cetacean Res. Manag.* **8**, 145–159 (2006).
11. H. C. Martin, E. M. Batty, J. Hussin, P. Westall, T. Daish, S. Kolomyjec, P. Piazza, R. Bowden, M. Hawkins, T. Grant, C. Moritz, F. Grutzner, J. Gongora, P. Donnelly, Insights into Platypus Population Structure and History from Whole-Genome Sequencing. *Mol. Biol. Evol.* **35**, 1238–1252 (2018).
12. E. M. Koch, R. M. Schweizer, T. M. Schweizer, D. R. Stahler, D. W. Smith, R. K. Wayne, J. Novembre, De Novo Mutation Rate Estimation in Wolves of Known Pedigree. *Mol. Biol. Evol.* **36**, 2536–2547 (2019).
13. L. Smeds, A. Qvarnström, H. Ellegren, Direct estimate of the rate of germline mutation in a bird. *Genome Res.* **26**, 1211–1218 (2016).
14. T. R. Frasier, S. D. Petersen, L. Postma, L. Johnson, M. P. Heide-Jørgensen, S. H. Ferguson, Abundance estimation from genetic mark-recapture data when not all sites are sampled: An example with the bowhead whale. *Glob. Ecol. Conserv.* **22**, e00903 (2020).
15. Y. V. Bukhman, P. A. Morin, S. Meyer, L.-F. (Jack) Chu, J. K. Jacobsen, J. Antosiewicz-Bourget, D. Mamott, M. Gonzales, C. Argus, J. Bolin, M. E. Berres, O. Fedrigo, J. Steill, S. A. Swanson, P. Jiang, A. Rhie, G. Formenti, A. M. Phillippy, R. S. Harris, J. M. D. Wood, K. Howe, B. Kirilenko, C. Munegowda, M. Hiller, A. Jain, D. Kihara, J. S. Johnston, A. Ionkov, K. Raja, H. Toh, A. Lang, M. Wolf, E. Jarvis, J. A. Thomson, M. J. P. Chaisson, R. Stewart, A high-quality blue whale genome, segmental duplications, and historical demography (2022), , doi:10.21203/rs.3.rs-1910240/v1.
16. L. A. Bergeron, S. Besenbacher, J. Bakker, J. Zheng, P. Li, G. Pacheco, M.-H. S. Sinding, M. Kamilari, M. T. P. Gilbert, M. H. Schierup, G. Zhang, The germline mutational process in rhesus macaque and its implications for phylogenetic dating. *GigaScience*. **10**, giab029 (2021).
17. L. A. Bergeron, S. Besenbacher, T. Turner, C. J. Versoza, R. J. Wang, A. L. Price, E. Armstrong, M. Riera, J. Carlson, H. Chen, M. W. Hahn, K. Harris, A. S. Kleppe, E. H.

bioRxiv preprint doi: https://doi.org/10.1101/2022.10.06.510775; this version posted October 7, 2022. The copyright holder for this preprint (which was not certified by peer review) is the author/funder, who has granted bioRxiv a license to display the preprint in perpetuity. It is made available under aCC-BY-NC-ND 4.0 International license.

López-Nandam, P. Moorjani, S. P. Pfeifer, G. P. Tiley, A. D. Yoder, G. Zhang, M. H. Schierup, The Mutationathon highlights the importance of reaching standardization in estimates of pedigree-based germline mutation rates. *eLife*. **11**, e73577 (2022).

18. S. Besenbacher, C. Hvilsom, T. Marques-Bonet, T. Mailund, M. H. Schierup, Direct estimation of mutations in great apes reconciles phylogenetic dating. *Nat. Ecol. Evol.* **3**, 286–292 (2019).
19. H. Jónsson, P. Sulem, B. Kehr, S. Kristmundsdottir, F. Zink, E. Hjartarson, M. T. Hardarson, K. E. Hjorleifsson, H. P. Eggertsson, S. A. Gudjonsson, L. D. Ward, G. A. Arnadottir, E. A. Helgason, H. Helgason, A. Gylfason, A. Jonasdottir, A. Jonasdottir, T. Rafnar, M. Frigge, S. N. Stacey, O. Th. Magnusson, U. Thorsteinsdottir, G. Masson, A. Kong, B. V. Halldorsson, A. Helgason, D. F. Gudbjartsson, K. Stefansson, Parental influence on human germline *de novo* mutations in 1,548 trios from Iceland. *Nature*. **549**, 519–522 (2017).
20. A. Cagan, A. Baez-Ortega, N. Brzozowska, F. Abascal, T. H. H. Coorens, M. A. Sanders, A. R. J. Lawson, L. M. R. Harvey, S. Bhosle, D. Jones, R. E. Alcantara, T. M. Butler, Y. Hooks, K. Roberts, E. Anderson, S. Lunn, E. Flach, S. Spiro, I. Januszczak, E. Wrigglesworth, H. Jenkins, T. Dallas, N. Masters, M. W. Perkins, R. Deaville, M. Druce, R. Bogeska, M. D. Milsom, B. Neumann, F. Gorman, F. Constantino-Casas, L. Peachey, D. Bochynska, E. St. J. Smith, M. Gerstung, P. J. Campbell, E. P. Murchison, M. R. Stratton, I. Martincorena, Somatic mutation rates scale with lifespan across mammals. *Nature*. **604**, 517–524 (2022).
21. L. Nunney, Resolving Peto's paradox: Modeling the potential effects of size-related metabolic changes, and of the evolution of immune policing and cancer suppression. *Evol. Appl.* **13**, 1581–1592 (2020).
22. C. Haag-Liautard, N. Coffey, D. Houle, M. Lynch, B. Charlesworth, P. D. Keightley, Direct Estimation of the Mitochondrial DNA Mutation Rate in Drosophila melanogaster. *PLOS Biol.* **6**, e204 (2008).
23. M. Stoneking, Hypervariable sites in the mtDNA control region are mutational hotspots. *Am. J. Hum. Genet.* **67**, 1029–1032 (2000).
24. M. D. Hendy, M. D. Woodhams, A. Dodd, Modelling mitochondrial site polymorphisms to infer the number of segregating units and mutation rate. *Biol Lett*. **5**, 397–400 (2009).
25. M. del M. González, A. Ramos, M. P. Aluja, C. Santos, Sensitivity of mitochondrial DNA heteroplasmy detection using Next Generation Sequencing. *Mitochondrion*. **50**, 88–93 (2020).
26. C. D. Millar, A. Dodd, J. Anderson, G. C. Gibb, P. A. Ritchie, C. Baroni, M. D. Woodhams, M. D. Hendy, D. M. Lambert, Mutation and Evolutionary Rates in Adélie Penguins from the Antarctic. *PLoS Genet.* **4** (2008), doi:10.1371/journal.pgen.1000209.
27. B. Rebolledo-Jaramillo, M. Shu-Wei Su, N. Stoler, J. A. McElhoe, B. Dickins, D. Blankenberg, T. S. Korneliussen, F. Chiaromonte, R. Nielsen, M. M. Holland, I. M. Paul, A. Nekrutenko, K. D. Makova, Maternal age effect and severe germ-line bottleneck in the inheritance of human mitochondrial DNA. *Proc. Natl. Acad. Sci.* **111**, 15474–15479 (2014).
28. J. N. Wolff, D. J. White, M. Woodhams, H. E. White, N. J. Gemmell, The strength and timing of the mitochondrial bottleneck in salmon suggests a conserved mechanism in vertebrates. *PLoS ONE*. **6** (2011), doi:10.1371/journal.pone.0020522.
29. A. A. Zaidi, P. R. Wilton, M. Shu-Wei Su, I. M. Paul, B. Arbeithuber, K. Anthony, A. Nekrutenko, R. Nielsen, K. D. Makova, Bottleneck and selection in the germline and maternal age influence transmission of mitochondrial DNA in human pedigrees. *Proc. Natl. Acad. Sci.* **116**, 25172–25178 (2019).
30. K. Ruegg, H. C. Rosenbaum, E. C. Anderson, M. Engel, A. Rothschild, C. S. Baker, S. R. Palumbi, Long-term population size of the North Atlantic humpback whale within the context of worldwide population structure. *Conserv. Genet.* **14**, 103–114 (2013).
31. P. Stevick, J. Allen, P. Clapham, N. Friday, S. Katona, F. Larsen, J. Lien, D. Mattila, P. Palsbøll, J. Sigurjónsson, T. Smith, N. Øien, P. Hammond, North Atlantic humpback whale abundance and rate of increase four decades after protection from whaling. *Mar.*

bioRxiv preprint doi: https://doi.org/10.1101/2022.10.06.510775; this version posted October 7, 2022. The copyright holder for this preprint (which was not certified by peer review) is the author/funder, who has granted bioRxiv a license to display the preprint in perpetuity. It is made available under aCC-BY-NC-ND 4.0 International license.

Ecol. Prog. Ser. **258**, 263–273 (2003).
32. M. D. Kessler, D. P. Loesch, J. A. Perry, N. L. Heard-Costa, D. Taliun, B. E. Cade, H. Wang, M. Daya, J. Ziniti, S. Datta, J. C. Celedón, M. E. Soto-Quiros, L. Avila, S. T. Weiss, K. Barnes, S. S. Redline, R. S. Vasan, A. D. Johnson, R. A. Mathias, R. Hernandez, J. G. Wilson, D. A. Nickerson, G. Abecasis, S. R. Browning, S. Zöllner, J. R. O'Connell, B. D. Mitchell, National Heart, Lung, and Blood Institute Trans-Omics for Precision Medicine (TOPMed) Consortium, TOPMed Population Genetics Working Group,, T. D. O'Connor, De novo mutations across 1,465 diverse genomes reveal mutational insights and reductions in the Amish founder population. *Proc. Natl. Acad. Sci.* **117**, 2560–2569 (2020).
33. P. J. Palsbøll, F. Larsen, E. S. Hansen, Sampling of skin biopsies from free-ranging large cetaceans at West Greenland: development of new designs. *IWC Workshop Pap.*, 1–8 (1991).
34. B. Amos, A. R. Hoelzel, Long-term skin preservation of whale skin for DNA analysis. *Rep Int Whal. Comm Spec Issue*. **13**, 99–103 (1991).
35. D. W. Russel, J. Sambrook, *Molecular cloning: a laboratory manual* (Cold Spring Harbor, NY: Cold Spring Harbor Laboratory., 2001).
36. M. Berube, P. Palsbøll, Identification of sex in Cetaceans by multiplexing with three ZFX and ZFY specific primers. *Mol. Ecol.* **5**, 283–287 (1996).
37. H. Li, Aligning sequence reads, clone sequences and assembly contigs with BWA-MEM (2013), (available at http://arxiv.org/abs/1303.3997).
38. Broad-Institute, Picard, (available at https://broadinstitute.github.io/picard/).
39. A. Mckenna, M. Hanna, E. Banks, A. Sivachenko, K. Cibulskis, A. Kernytsky, K. Garimella, D. Altshuler, S. Gabriel, M. Daly, M. A. Depristo, The Genome Analysis Toolkit: A MapReduce framework for analyzing next-generation DNA sequencing data. *Genome Res.* **20**, 1297–1303 (2010).
40. P. Danecek, A. Auton, G. Abecasis, C. A. Albers, E. Banks, M. A. Depristo, R. E. Handsaker, G. Lunter, G. T. Marth, S. T. Sherry, G. Mcvean, R. Durbin, G. Project, The variant call format and VCFtools. *Bioinformatics*. **27**, 2156–2158 (2011).
41. L. Maretty, J. M. Jensen, B. Petersen, J. A. Sibbesen, S. Liu, P. Villesen, L. Skov, K. Belling, C. Theil Have, J. M. G. Izarzugaza, M. Grosjean, J. Bork-Jensen, J. Grove, T. D. Als, S. Huang, Y. Chang, R. Xu, W. Ye, J. Rao, X. Guo, J. Sun, H. Cao, C. Ye, J. van Beusekom, T. Espeseth, E. Flindt, R. M. Friborg, A. E. Halager, S. Le Hellard, C. M. Hultman, F. Lescai, S. Li, O. Lund, P. Løngren, T. Mailund, M. L. Matey-Hernandez, O. Mors, C. N. S. Pedersen, T. Sicheritz-Pontén, P. Sullivan, A. Syed, D. Westergaard, R. Yadav, N. Li, X. Xu, T. Hansen, A. Krogh, L. Bolund, T. I. A. Sørensen, O. Pedersen, R. Gupta, S. Rasmussen, S. Besenbacher, A. D. Børglum, J. Wang, H. Eiberg, K. Kristiansen, S. Brunak, M. H. Schierup, Sequencing and de novo assembly of 150 genomes from Denmark as a population reference. *Nature*. **548**, 87–91 (2017).
42. J. Ye, G. Coulouris, I. Zaretskaya, I. Cutcutache, S. Rozen, T. L. Madden, Primer-BLAST: A tool to design target-specific primers for polymerase chain reaction. *BMC Bioinformatics*. **13**, 134 (2012).
43. N. Jullien, AmplifX 1.7. 0. (2013).
44. E. Werle, C. Schneider, M. Renner, M. Völker, W. Fiehn, Convenient single-step, one tube purification of PCR products for direct sequencing. *Nucleic Acids Res.* **22**, 4354–4355 (1994).
45. P. Cingolani, A. Platts, L. L. Wang, M. Coon, T. Nguyen, L. Wang, S. J. Land, X. Lu, D. M. Ruden, A program for annotating and predicting the effects of single nucleotide polymorphisms, SnpEff. *Fly (Austin)*. **6**, 80–92 (2012).
46. M. Bérubé, M. B. Rew, H. Skaug, H. Jørgensen, J. Robbins, P. Best, R. Sears, P. J. Palsbøll, Polymorphic microsatellite loci isolated from humpback whale, Megaptera novaeangliae and fin whale, balaenoptera physalus. *Conserv. Genet.* **6**, 631–636 (2005).
47. E. Valsecchi, W. Amos, Microsatellite markers for the study of cetacean populations. *Mol. Ecol.* **5**, 151–156 (1996).

bioRxiv preprint doi: https://doi.org/10.1101/2022.10.06.510775; this version posted October 7, 2022. The copyright holder for this preprint (which was not certified by peer review) is the author/funder, who has granted bioRxiv a license to display the preprint in perpetuity. It is made available under aCC-BY-NC-ND 4.0 International license.

48. P. J. Palsbøll, M. Bérubé, A. H. Larsen, H. Jørgensen, Primers for the amplification of tri- and tetramer microsatellite loci in baleen whales. *Mol. Ecol.* **6**, 893–5 (1997).
49. M. Bérubé, A. Aguilar, D. Dendanto, F. Larsen, G. di S. Notarbartolo, R. Sears, J. Sigurjónsson, J. Urban-R, P. J. Palsbøll, Population genetic structure of North Atlantic, Mediterranean Sea and Sea of Cortez fin whales, Balaenoptera physalus (Linnaeus 1758): analysis of mitochondrial and nuclear loci. *Mol. Ecol.* **7**, 585–599 (1998).
50. M. Bérubé, H. Jørgensen, R. McEwing, P. J. Palsbøll, Polymorphic di-nucleotide microsatellite loci isolated from the humpback whale, Megaptera novaeangliae. *Mol. Ecol.* **9**, 2181–3 (2000).
51. M. B. Rew, J. Robbins, D. Mattila, P. J. Palsbøll, M. Bérubé, How many genetic markers to tag an individual? An empirical assessment of false matching rates among close relatives. *Ecol. Appl.* **21**, 877–887 (2011).
52. P. J. Palsbøll, P. J. Clapham, D. K. Mattila, F. Larsen, R. Sears, H. R. Siegismund, J. Sigurjónsson, O. Vasquez, P. Arctander, Distribution of mtDNA haplotypes in North Atlantic humpback whales: the influence of behaviour on population structure. *Mar. Ecol. Prog. Ser.* **116**, 1–10 (1995).
53. V. Drouot, M. Bérubé, A. Gannier, J. C. Goold, R. J. Reid, P. J. Palsbøll, A note on genetic isolation of Mediterranean sperm whales (Physeter macrocephalus) suggested by mitochondrial DNA. *J. Cetacean Res. Manag.* **6**, 29–32 (2004).
54. U. Arnason, A. Gullberg, B. Widegren, Cetacean mitochondrial DNA control region: sequences of all extant baleen whales and two sperm whale species. *Mol. Biol. Evol.* **10**, 960–70 (1993).
55. K. B. Mullis, F. A. Faloona, Specific synthesis of DNA in vitro via a polymerase-catalyzed chain reaction. *Methods Enzymol.* **155**, 335–350 (1987).
56. S. K. Katona, H. P. Whitehead, Identifying Humpback Whales using their natural markings. *Polar Rec.* **20**, 439–439 (1981).
57. P. J. Clapham, C. A. Mayo, Reproduction and recruitment of individually identified humpback whales, Megaptera novaeangliae, observed in Massachusetts Bay, 1979–1985. *Can. J. Zool.* **65**, 2853–2863 (1987).
58. M. Riester, P. F. Stadler, K. Klemm, FRANz: reconstruction of wild multi-generation pedigrees. **25**, 2134–2139 (2009).
59. M. Suarez-Menendez, V. Rivera-Leon, J. Robbins, M. Bérubé, P. J. Palsbøll, PHFinder: Assisted detection of point heteroplasmy in Sanger sequencing chromatograms (2022), p. 2022.08.17.501710, , doi:10.1101/2022.08.17.501710.
60. T. Sasaki, M. Nikaido, H. Hamilton, M. Goto, H. Kato, N. Kanda, L. A. Pastene, Y. Cao, R. E. Fordyce, M. Hasegawa, N. Okada, Mitochondrial Phylogenetics and Evolution of Mysticete Whales. *Syst. Biol.* **54**, 77–90 (2005).
61. B. Langmead, S. L. Salzberg, Fast gapped-read alignment with Bowtie 2. *Nat. Methods*. **9**, 357–9 (2012).
62. H. Li, B. Handsaker, A. Wysoker, T. Fennell, J. Ruan, N. Homer, G. Marth, G. Abecasis, R. Durbin, G. Project, D. P. Subgroup, The Sequence Alignment/Map format and SAMtools. *Bioinformatics*. **25**, 2078–2079 (2009).
63. A. R. Quinlan, I. M. Hall, BEDTools: a flexible suite of utilities for comparing genomic features. *Bioinforma. Appl. NOTE*. **26**, 841–842 (2010).
64. A. Morgulis, E. M. Gertz, A. A. Schäffer, R. Agarwala, A fast and symmetric DUST implementation to mask low-complexity DNA sequences. *J. Comput. Biol.* **13**, 1028–1040 (2006).
65. P. J. A. Cock, T. Antao, J. T. Chang, B. A. Chapman, C. J. Cox, A. Dalke, I. Friedberg, T. Hamelryck, F. Kauff, B. Wilczynski, M. J. L. de Hoon, Biopython: freely available Python tools for computational molecular biology and bioinformatics. *Bioinformatics*. **25**, 1422–1423 (2009).
66. H. Li, J. Barrett, A statistical framework for SNP calling, mutation discovery, association mapping and population genetical parameter estimation from sequencing data. *Bioinformatics*. **27**, 2987–2993 (2011).
67. M. del M. González, A. Ramos, M. P. Aluja, C. Santos, Sensitivity of mitochondrial DNA

bioRxiv preprint doi: https://doi.org/10.1101/2022.10.06.510775; this version posted October 7, 2022. The copyright holder for this preprint (which was not certified by peer review) is the author/funder, who has granted bioRxiv a license to display the preprint in perpetuity. It is made available under aCC-BY-NC-ND 4.0 International license.

heteroplasmy detection using Next Generation Sequencing. *Mitochondrion*. **50**, 88–93 (2020).
68. B. Rebolledo-Jaramillo, M. Shu-Wei Su, N. Stoler, J. A. McElhoe, B. Dickins, D. Blankenberg, T. S. Korneliussen, F. Chiaromonte, R. Nielsen, M. M. Holland, I. M. Paul, A. Nekrutenko, K. D. Makova, Maternal age effect and severe germ-line bottleneck in the inheritance of human mitochondrial DNA. *Proc. Natl. Acad. Sci.* **111**, 15474–15479 (2014).
69. J. N. Wolff, D. J. White, M. Woodhams, H. E. White, N. J. Gemmell, The Strength and Timing of the Mitochondrial Bottleneck in Salmon Suggests a Conserved Mechanism in Vertebrates. *PLoS ONE*. **6**, 20522–20522 (2011).
70. L. M. Cree, ; D C Samuels, ; S C De, S. Lopes, ; H K Rajasimha, ; P Wonnapinij, ; J R Mann, ; H H Dahl, ; P F Chinnery, L. M. Cree, D. C. Samuels, S. Chuva, H. K. Rajasimha, P. Wonnapinij, J. R. Mann, H.-H. M. Dahl, P. F. Chinnery, "A reduction of mitochondrial DNA molecules during embryogenesis explains the rapid segregation of genotypes A reduction in the number of mitochondrial DNA molecules during embryogenesis explains the rapid segregation of genotypes" (2008), pp. 249–54.
71. M. D. Hendy, M. D. Woodhams, A. Dodd, Modelling mitochondrial site polymorphisms to infer the number of segregating units and mutation rate. *Biol. Lett.* **5**, 397–400 (2009).
72. J. Roman, S. R. Palumbi, Whales Before Whaling in the North Atlantic. *Science*. **301**, 508–510 (2003).
73. P. J. Clapham, M. Bérubé, D. K. Mattila, Sex Ratio of the Gulf of Maine Humpback Whale Population. *Mar. Mammal Sci.* **11**, 227–231 (1995).
74. L. Nunney, The Influence of Mating System and Overlapping Generations on Effective Population Size. *Evolution*. **47**, 1329–1341 (1993).
75. R. G. Chittleborough, Dynamics of two populations of the humpback whale, Megaptera novaeangliae (Borowski). *Mar. Freshw. Res.* **16**, 33–128 (1965).
76. C. Feng, M. Pettersson, S. Lamichhaney, C.-J. Rubin, N. Rafati, M. Casini, A. Folkvord, L. Andersson, Moderate nucleotide diversity in the Atlantic herring is associated with a low mutation rate. *eLife*. **6**, e23907 (2017).
77. M. Malinsky, H. Svardal, A. M. Tyers, E. A. Miska, M. J. Genner, G. F. Turner, R. Durbin, Whole-genome sequences of Malawi cichlids reveal multiple radiations interconnected by gene flow. *Nat. Ecol. Evol.* **2**, 1940–1955 (2018).
78. M. Zhang, Q. Yang, H. Ai, L. Huang, Revisiting the evolutionary history of pigs via De Novo mutation rate estimation in a three-generation pedigree. *Genomics Proteomics Bioinformatics* (2022), doi:10.1016/j.gpb.2022.02.001.
79. S. J. Lindsay, R. Rahbari, J. Kaplanis, T. Keane, M. E. Hurles, Similarities and differences in patterns of germline mutation between mice and humans. *Nat. Commun.* **10**, 4053 (2019).
80. C. Yang, Y. Zhou, S. Marcus, G. Formenti, L. A. Bergeron, Z. Song, X. Bi, J. Bergman, M. M. C. Rousselle, C. Zhou, L. Zhou, Y. Deng, M. Fang, D. Xie, Y. Zhu, S. Tan, J. Mountcastle, B. Haase, J. Balacco, J. Wood, W. Chow, A. Rhie, M. Pippel, M. M. Fabiszak, S. Koren, O. Fedrigo, W. A. Freiwald, K. Howe, H. Yang, A. M. Phillippy, M. H. Schierup, E. D. Jarvis, G. Zhang, Evolutionary and biomedical insights from a marmoset diploid genome assembly. *Nature*. **594**, 227–233 (2021).
81. E. M. Koch, R. M. Schweizer, T. M. Schweizer, D. R. Stahler, D. W. Smith, R. K. Wayne, J. Novembre, De Novo Mutation Rate Estimation in Wolves of Known Pedigree. *Mol. Biol. Evol.* **36**, 2536–2547 (2019).
82. F. L. Wu, A. I. Strand, L. A. Cox, C. Ober, J. D. Wall, P. Moorjani, M. Przeworski, A comparison of humans and baboons suggests germline mutation rates do not track cell divisions. *PLOS Biol.* **18**, e3000838 (2020).
83. G. W. C. Thomas, R. J. Wang, A. Puri, R. A. Harris, M. Raveendran, D. S. T. Hughes, S. C. Murali, L. E. Williams, H. Doddapaneni, D. M. Muzny, R. A. Gibbs, C. R. Abee, M. R. Galinski, K. C. Worley, J. Rogers, P. Radivojac, M. W. Hahn, Reproductive Longevity Predicts Mutation Rates in Primates. *Curr. Biol.* **28**, 3193-3197.e5 (2018).

bioRxiv preprint doi: https://doi.org/10.1101/2022.10.06.510775; this version posted October 7, 2022. The copyright holder for this preprint (which was not certified by peer review) is the author/funder, who has granted bioRxiv a license to display the preprint in perpetuity. It is made available under aCC-BY-NC-ND 4.0 International license.

84. R. J. Wang, Y. Peña-Garcia, M. G. Bibby, M. Raveendran, R. A. Harris, H. T. Jansen, C. T. Robbins, J. Rogers, J. L. Kelley, M. W. Hahn, Examining the effects of hibernation on germline mutation rates in grizzly bears. *Genome Biol. Evol.*, evac148 (2022).
85. R. J. Wang, M. Raveendran, R. A. Harris, W. J. Murphy, L. A. Lyons, J. Rogers, M. W. Hahn, De novo Mutations in Domestic Cat are Consistent with an Effect of Reproductive Longevity on Both the Rate and Spectrum of Mutations. *Mol. Biol. Evol.* **39**, msac147 (2022).
86. S. P. Pfeifer, Direct estimate of the spontaneous germ line mutation rate in African green monkeys. *Evolution*. **71**, 2858–2870 (2017).
87. S. Besenbacher, C. Hvilsom, T. Marques-Bonet, T. Mailund, M. H. Schierup, Direct estimation of mutations in great apes reconciles phylogenetic dating. *Nat. Ecol. Evol.* **3**, 286–292 (2019).
88. C. Harland, C. Charlier, L. Karim, N. Cambisano, M. Deckers, M. Mni, E. Mullaart, W. Coppieters, M. Georges, Frequency of mosaicism points towards mutation-prone early cleavage cell divisions in cattle (2017), p. 079863.
89. C. R. Campbell, G. P. Tiley, J. W. Poelstra, K. E. Hunnicutt, P. A. Larsen, H.-J. Lee, J. L. Thorne, M. dos Reis, A. D. Yoder, Pedigree-based and phylogenetic methods support surprising patterns of mutation rate and spectrum in the gray mouse lemur. *Heredity*. **127**, 233–244 (2021).